




Evaluation of the switching rate for magnetic nanoparticles: Analysis, optimization, and comparison of various numerical simulation algorithms

Elena K. Semenova , Dmitry V. Berkov , and Natalia L. Gorn
General Numerics Research Lab, Moritz-von-Rohr-Straße 1A, D-07745 Jena, Germany

 (Received 4 August 2020; revised 22 September 2020; accepted 23 September 2020; published 14 October 2020)

In this paper, we present a detailed comparative study of various analytical and numerical methods intended for the evaluation of the escape rate over high-energy barriers (transition rate or, equivalently, switching times) in magnetic systems, using the archetypal application-relevant model of a biaxial macrospin. First, we derive a closed-form analytical expression of the transition rate for such a particle, using the general formalism of Dejardin *et al.* [*Phys. Rev. E* **63**, 021102 (2001)], and define a parameter which determines whether the system is in the low, intermediate, or high damping regimes. Then we carry out a comprehensive analysis of three numerical algorithms: time-temperature extrapolation method, “energy bounce” methods [S. Wang and P. Visscher, *J. Appl. Phys.* **99**, 08G106 (2006)], and the forward-flux sampling [R. J. Allen *et al.*, *Phys. Rev. Lett.* **94**, 018104 (2005)], which appear to be the most promising candidates for evaluating the transition rate using computer simulations. Based on underlying physical principles and peculiarities of magnetic moment systems, we suggest several optimization possibilities, which strongly improve the performance of these methods for our applications. For energy barriers ΔE in the range $10k_B T \leq \Delta E \leq 60k_B T$ we compare the switching times, which correspondingly span more than 20 orders of magnitude, obtained with all the above-mentioned analytical and numerical techniques. We show that although for relatively small barriers all methods agree well with each other (and with straightforward Langevin dynamics simulations), for larger barriers the differences become significant, so that only the forward-flux method provides physically reasonable results, giving switching times which exceed the prediction of analytical approaches (interestingly, the ratio $\tau_{sw}^{FFS}/\tau_{sw}^{an}$ is nearly constant for a very broad interval of switching times). The reasons for the corresponding behavior of numerical methods are explained. Finally, we discuss the perspectives of the application of the analyzed numerical techniques to full-scale micromagnetic simulations, where the presence of several contributions to the total system energy makes the situation qualitatively different from that for the macrospin approach.

DOI: [10.1103/PhysRevB.102.144419](https://doi.org/10.1103/PhysRevB.102.144419)

I. INTRODUCTION

During the recent two decades, a large progress by the evaluation of escape rates over high-energy barriers in different physical systems in general and in magnetic systems in particular has been achieved. First of all, for systems of magnetic particles with and without internal magnetization structure several methods for computing the height of energy barriers separating their metastable energy minima have been implemented: minimization of the Onsager-Machlup functional [1] for an interacting system of single-domain particles [2], string method searching for the “minimal energy path” based on the condition that the energy gradient component perpendicular to this path should be zero along the whole path [3], and the closely related “nudged elastic band” (NEB) method [4]. The latter method, which is presently the most widely used, is the “micromagnetic” adaptation of the NEB algorithm of Jonsson *et al.* [5], with the main idea to connect the neighboring system states along the transition path with artificial “springs” to prevent a too large distance between these states during the path-finding procedure.

However, knowledge of the energy barrier ΔE alone is obviously not enough to compute the average lifetime of a

system within an energy well (or, correspondingly, the escape rate Γ out of this well), the quantity of real interest for applications. The simplest possibility to evaluate this rate is provided by the Arrhenius law $\Gamma = \nu_{att} \exp(\Delta E/k_B T)$, where the “attempt frequency” ν_{att} is usually interpreted as the oscillation frequency of the system near the energy minimum. The evaluation of this frequency by itself for systems with an internal magnetization structure is a highly nontrivial task due to the existence of internal eigenmodes in such systems (see, e.g., [6,7]). But, even with the properly evaluated ν_{att} , the Arrhenius formula can not be considered as a satisfactory approach from a fundamental point of view, as stressed, e.g., in [8,9], because it does not contain a dependence of the switching rate on the system damping, which is mandatory according to the fluctuation-dissipation theorem.

The problem of providing an analytical expression of the escape rate, which would explicitly contain the damping parameter, was first solved in the intermediate-to-high damping (IHD) regime by Brown [10] and later for very low damping (VLD) by Klik and Günther [11]. In the meantime, the correct analytical description of the escape rate for a system with an arbitrary damping was provided in the classical paper of Mel'nikov and Meshkov [12], who have evaluated both the

lifetime of a Brownian particle in a single energy well and decay rates in a double-well potential in the corresponding general case. The formalism and ideas from [11,12] were successfully applied to a single-domain magnetic particle in [13,14], resulting in an analytical formula for the escape rate out of a single well and transition rates between two energy minima in a double-well magnetic system valid for all damping regimes. The comprehensive treatment of this topic can be found in the extensive review [9].

Although very useful, this analytical approach has several limitations. Even for single-domain particles, the method cannot take into account the so-called “back-hopping” trajectories, where the system magnetization returns back to the initial local minimum shortly after crossing the saddle point, i.e., without reaching the (partial) thermodynamic equilibrium in the target minimum. Further, for magnetic systems with a symmetry lower than the perfect uniaxial anisotropy with two equivalent minima, as it is the case, e.g., for particles in an external field (both along the easy axis [15] and oblique [16]), or for particles with the anisotropy more complicated than a uniaxial one [17], the treatment becomes increasingly complicated, making corresponding final expressions difficult in practical applications.

The really serious problem of the analytical treatment, however, is that it cannot be applied to most application-relevant cases, where the particle size is larger than either the exchange or demagnetizing characteristic micromagnetic length (for corresponding definitions and discussion see, e.g., [18]). For such systems, magnetization configuration becomes spatially nonhomogeneous, thus making the usage of analytical methods nearly impossible. For this reason, there exists a pressing demand for numerical methods computing not only the energy barrier, but the actual escape rate. Straightforward Langevin dynamics (LD), being a powerful tool for short-time simulations (see, e.g., [19–23], is obviously not applicable for studying magnetization transitions between minima separated by high-energy barriers (about $\Delta E > 10k_B T$) because waiting times become macroscopically large.

Numerical methods for evaluating the escape rate in systems with high barriers usually employ the paradigm of a “gradual climbing” uphill the energy surface by computing the probability $p(\lambda_{i-1} \rightarrow \lambda_i)$ to reach some intermediate interface λ_i from the previous interface λ_{i-1} . The subsequent interfaces should be positioned relatively close to each other, either in the coordinate space or in the energy space, so that $p(\lambda_{i-1} \rightarrow \lambda_i)$ can be computed reasonably fast and accurately by standard LD simulations. Multiplication of these transition probabilities for all interface pairs between the two energy minima of interest should give (augmented by a properly defined factor with the dimensionality $1/t$) the total transition rate.

The most successful general-purpose representative of the methods outlined above is the forward-flux sampling (FFS) (see [24–26] for specific issues and [27] for a comprehensive review). In FFS, the interfaces are defined in the coordinate space, usually by setting the desired values of the so-called “reaction coordinate” or an “order parameter,” which value defines whether the transition has occurred or not. In micromagnetics, this method was applied for two very specific

systems in [28,29]. A related method, where the interfaces were defined as the system energy values used to confine the magnetization motion, is the “energy bounce” algorithm introduced in [30]; this short paper contains only the basic idea and the application example to a macrospin with only one value of the energy barrier.

Hence, it can be seen that as far as micromagnetic applications are considered, the methods for computing transition rates over high barriers are at their infancy (what can be seen already from a very small number of corresponding publications). Physical understanding of their functioning when applied to micromagnetic simulations is insufficient, systematic comparison of corresponding numerical results with the available analytical expressions is, up to our knowledge, not available, and the optimization of the algorithms with respect to the minimization of the computational time (what is crucial for such time-consuming simulations) has not been accomplished. Further, the analysis of possible alternative algorithms capable of computing the switching time without a gradual climbing from the minimum to the saddle point has also not been performed.

In our study, we intend to fill in the gaps outlined above, performing detailed analytical and numerical studies of magnetization transitions over energy barriers. We confine our study to purely classical processes, leaving aside the phenomenon of macroscopic quantum tunneling of magnetization; the latter is usually relevant at very low temperatures (according to various estimations, for $T < T_{qt}$, where $T_{qt} \sim 100 \text{ mK} \div 10 \text{ K}$ [31,32]), which are of no interest for applications we have in mind. This paper is organized as follows: In Sec. II we describe our biaxial macrospin model and derive closed-form analytical expressions for its switching rate both in the Arrhenius approximation and in the general formalism [13,14] for an arbitrary damping value. In Sec. III we present results of LD simulations, to be used as a reference for further comparisons. In this section we also discuss in detail a very important question of distinguishing between “false” and “true” transitions, when the magnetization projection of interest changes its sign. In Sec. IV we present the most straightforward method for computing switching rates for a system with arbitrarily high barriers using only LD simulations, our “time-temperature” extrapolation method (related to the idea suggested in [33]). In this method we use the extrapolation of switching rates obtained at several higher temperatures toward the room temperature to obtain the desired quantity. Next, in Sec. V, we perform the detailed analysis of the energy bounce method (EBM) and introduce two versions of this method, which enable to strongly reduce the corresponding computation time and to prepare EBM for usage in full-scale micromagnetic simulations. In addition, we discuss again the criterion for filtering out the false switchings, as the dynamics in EBM is qualitatively different from that by unconstrained LD simulations. Section VI is devoted to our implementation of the FFS method, where we suggest the placement of interfaces in the energy space (instead of using magnetization projections), allowing us to obtain the best interface positions without any optimization, thus greatly increasing the statistical accuracy of results. Finally, in Sec. VII we compare the results obtained by all analytical and numerical methods used in our study for energy barriers in

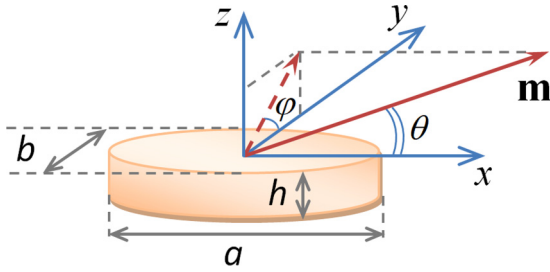


FIG. 1. Coordinate system and geometry of simulated nanoelements.

the interval $10k_B T \leq \Delta E \leq 60k_B T$, so that the corresponding switching times span over 20 orders of magnitude. In the Conclusion, we summarize our findings and discuss the comparative quality of the studied methods and perspectives of their application of all methods to full-scale micromagnetic simulations.

II. SIMULATED MODEL AND ANALYTICAL APPROXIMATIONS FOR THE ESCAPE RATE

A. Macrospin approximation (MSA)

In this study, we simulate magnetization switching of elliptical nanoelements with the thickness $h = 3$ nm, the short axis $b = 40$ nm, and different long axes $a = 50\text{--}100$ nm. Corresponding geometry together with Cartesian coordinates assumed throughout the paper is shown in Fig. 1. We use magnetization $M_s = 800$ G and Gilbert damping $\lambda = 0.01$ and neglect the magnetocrystalline anisotropy (magnetic parameters typical for Py). Shape anisotropy is introduced in the standard way via the demagnetizing field tensor \hat{N} with diagonal components N_x , N_y , and N_z [23]; in our geometry, we always have $N_x < N_y < N_z$. For all methods presented below, we have determined the transition rate at room temperature ($T = 300$ K).

In our simulations we use the macrospin approximation, i.e., we assume that the magnetization of nanoellipses is homogeneous in space and can only rotate as a whole. We point out that from the physical point of view this approximation is not valid for nanoelements of these sizes, because at least the long axis of our ellipses greatly exceeds the single-domain particle size for Py, which is estimated to be ~ 10 nm. However, we shall employ the macrospin model in order to focus our study on fundamental questions important for all methods intended for simulation of thermally activated switching, without yet being involved into the complicated problems related to *internal* dynamic modes of a switching system; corresponding problems (arising by the application of methods discussed below to full-scale micromagnetic simulations) will be discussed in Sec. VII.

From the four standard contributions to the micromagnetic energy (energy in an external field, magnetocrystalline anisotropy, exchange and magnetodipolar energy), only two terms are present in frames of MSA: energy in an external field and the magnetodipolar energy, which in this approximation is usually called the shape anisotropy energy. The first term is absent in our case, as we study magnetization switching without an external field. The shape anisotropy energy

is defined using the above-mentioned tensor \hat{N} and Cartesian components of the unit magnetization vector \mathbf{m} as

$$E_{\text{an}} = 2\pi M_s^2 V (N_x m_x^2 + N_y m_y^2 + N_z m_z^2), \quad (1)$$

where V denotes the particle volume. Expression (1) (biaxial anisotropy) is the simplest analytical approximation for the shape anisotropy energy of a flat elliptical magnetic nanoelements shown in Fig. 1; this shape is widely used for many applications including, e.g., in-plane magnetic random access memory (MRAM) cells. In addition, this is the simplest possible model where one has the easy-plane anisotropy (with $0xy$ as the easy plane) and the energy barrier between the two equilibrium states in this plane, along $+x$ and $-x$ directions.

For analytical calculations of the switching rate, we shall need the expansion of the density of this energy ($\epsilon = E/V$) near the energy minima (where $m_x = \pm 1$) and the saddle points (in-plane switching, hence, $m_y = \pm 1$) in terms of two remaining magnetization projections. Using the relation $m_x^2 + m_y^2 + m_z^2 = 1$ for the elimination of m_x in the first case and m_y in the second case, we obtain

$$\epsilon_{\text{min}}(\mathbf{m}) = \epsilon_{\text{min}}^{(0)} + 2\pi M_s^2 (C_{yx} m_y^2 + C_{zx} m_z^2), \quad (2)$$

$$\epsilon_{\text{sad}}(\mathbf{m}) = \epsilon_{\text{sad}}^{(0)} + 2\pi M_s^2 (C_{xy} m_x^2 + C_{zy} m_z^2), \quad (3)$$

where $C_{\alpha\beta} = N_\alpha - N_\beta$ ($\alpha, \beta = x, y, z$); note that our constants $C_{\alpha\beta}$ differ from the analogous constants c_i in [9] by the factor $4\pi M_s^2$.

In this paper we shall study the escape rate from the minimum corresponding to $m_x = +1$ (the region around this starting point is denoted as the basin **A**) to the minimum with $m_x = -1$ (with the surrounding region denoted as the basin **B**).

For the analysis of the behavior of different numerical methods, we shall need the density of states (number of states per unit energy interval) $D(E)$. Analytical evaluation of this dependence for a macrospin with a biaxial anisotropy is very tedious. For this reason, we have computed $D(E)$ numerically by evaluating the system energy (1) for all moment orientations on the (θ, ϕ) grid in the spherical coordinate system shown in Fig. 1, with the polar axis along the x axis and the azimuthal axis $\phi = 0$, along the y axis of our coordinate system. Correspondingly weighted ($w \propto \sin \theta$) energy values were assembled to a histogram. Resulting (normalized) $D(E)$ for several macrospin sizes are shown in Fig. 2. Note that the density of states for a biaxial macrospin diverges at the saddle-point energy $E_{\text{sad}} = E(\theta = \pi/2, \phi = 0 \text{ or } \pi)$ (because at this point both partial energy derivatives are zero: $\partial E/m_x = \partial E/m_z = 0$); however, this divergence is not as strong as for a uniaxial macrospin, where the saddle on the energy surface is represented by the whole line $\theta = \pi/2$.

In terms of this density of states, the probability $p(E)$ to observe an energy E for a system in thermodynamic equilibrium is

$$p(E) = D(E) e^{-E/k_B T}. \quad (4)$$

B. Arrhenius approximation of the escape rate

As mentioned in the Introduction, the simplest (and still most widely used) analytical approximation for the escape

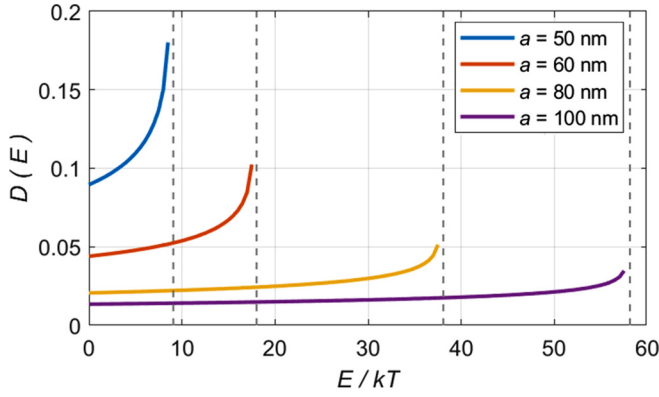


FIG. 2. Densities of states $D(E)$ for macrospins with various long ellipse axis a as shown in the legend.

rate resulting from the Arrhenius law is called the transition state theory rate [34]:

$$\Gamma^{\text{Arr}} = \frac{\omega_{\text{att}}}{2\pi} e^{-\Delta E/k_B T} \quad (5)$$

(k is Boltzmann constant). In MSA, both the energy barrier ΔE and the attempt frequency ω_{att} entering this expression can be evaluated analytically:

$$\Delta E = KV = 2\pi M_s^2 C_{yx} \frac{\pi hab}{4}, \quad (6)$$

$$\omega_{\text{att}} = \gamma 4\pi M_s \sqrt{C_{yx} C_{zx}} \quad (7)$$

(for the last expression see, e.g., [35]), where γ is the gyromagnetic ratio.

Dependencies of these quantities on the long axis of our elliptical nanoelement are shown in Fig. 3. Demagnetizing factors required in (6) and (7) have been computed in our paper [23] by comparing initial slopes of the hysteresis loop calculated by full-scale micromagnetic simulations (using the cell size $2 \times 2 \text{ nm}^2$ in plane) with the corresponding slope expected in MSA. As explained in detail in [23], demagnetizing factors computed this way represent a better approximation

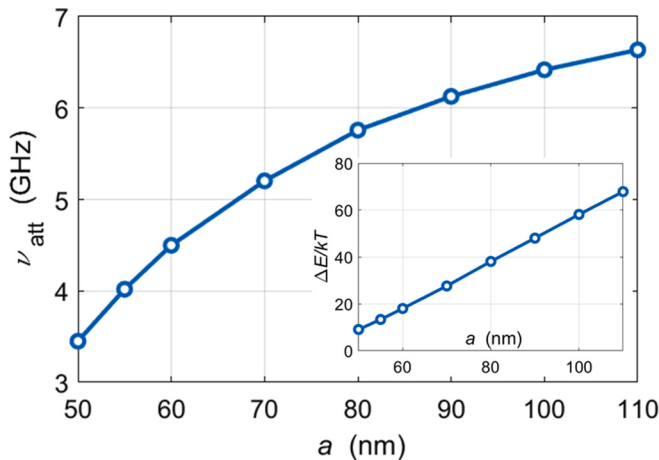


FIG. 3. Attempt frequency $\nu_{\text{att}} = \omega_{\text{att}}/2\pi$ (main plot) and energy barrier (6) (inset) as functions of the long ellipse axis a (short axis $b = 40 \text{ nm}$).

to the demagnetizing factors of a flat elliptical nanoelement than those computed from the axis ratios of the corresponding three-dimensional (3D) ellipsoid. Note that the dependence $\Delta E(a)$ is slightly nonlinear because demagnetizing coefficients $N_{x(y,z)}$ also depend of a ; however, this effect is weak compared to the linear dependence $V \sim a$.

The switching time in this approximation is

$$\tau_{\text{sw}}^{\text{Arr}} = \frac{1}{2\Gamma^{\text{Arr}}}, \quad (8)$$

where the additional factor $\frac{1}{2}$ is due to the existence of two saddle points in our system. Note that in the interval of the long axis lengths $a = 50\text{--}110 \text{ nm}$ studied here the switching time spans about 25 orders of magnitude. The dependence of $\log(\tau_{\text{sw}}^{\text{Arr}})$ vs a is also slightly nonlinear, not only due to the nonlinearity of $\Delta E(a)$, but also due to the nonlinear dependence $\nu_{\text{att}}(a)$ (see Fig. 3).

C. Magnetization escape rate for a biaxial particle by arbitrary damping

The Arrhenius expression has two well-known technical drawbacks: (i) it does not take into account the curvature of the energy landscape around the saddle point and (ii) it does not consider the possibility of a reverse transition shortly after the particle has crossed the energy barrier (back hopping). However, a much more serious problem is that the Arrhenius law does not include the damping constant, meaning that in this formalism the switching can occur without any damping, which is clearly impossible (no coupling to thermal bath present, see [8] for details). Large effort has been undertaken to derive physically meaningful expressions for various damping regimes [8,12,36]; corresponding results for the magnetic particle switching (where the precessional motion plays a very important role) have been summarized in the comprehensive review [9].

To proceed with our specific case, we shall need the general analytical expression for the magnetization escape rate Γ^{an} , valid (in the limit of the high-energy barrier $\Delta E \gg k_B T$) for all values of the damping parameter α [9,14]:

$$\Gamma^{\text{an}} = \frac{\Omega}{\omega_s} A(\alpha S) \Gamma^{\text{Arr}}, \quad \tau_{\text{sw}}^{\text{an}} = \frac{1}{2\Gamma^{\text{an}}}. \quad (9)$$

Here, the damped saddle angular frequency Ω

$$\Omega = \frac{\pi M_s^2 V}{k_B T} \frac{1}{\tau_N} \left[\sqrt{(C_{xy} - C_{zy})^2 - \frac{4C_{xy}C_{zy}}{\alpha^2}} - (C_{xy} + C_{zy}) \right] \quad (10)$$

[C_{xy} and C_{zy} are defined after the Eq. (3)] contains the characteristic diffusion time of the magnetization

$$\tau_N = \frac{VM_s}{2\gamma k_B T} \frac{1 + \alpha^2}{\alpha}. \quad (11)$$

The undamped saddle angular frequency ω_s is defined analogously to the attempt frequency (7):

$$\omega_s = \gamma 4\pi M_s \sqrt{-C_{xy} C_{zy}} \quad (12)$$

(note that $C_{xy} = N_x - N_y < 0$).

Prefactor A , called the depopulation factor because the decrease rate of the particle concentration within an energy minimum is proportional to A , has been derived in case of an arbitrary damping for the first time by Melnikov and Meshkov [12] and has the form

$$A(\alpha S) = \exp \left[\frac{1}{\pi} \int_0^\infty \ln \{ 1 - e^{-\alpha S(z^2+1/4)} \} \frac{dz}{z^2+1/4} \right]. \quad (13)$$

For small $\alpha \rightarrow 0$, the asymptotic behavior of this prefactor is $A(\alpha S) \rightarrow \alpha S$, so Eq. (9) reduces to the result of Klik and Gunther [11]. For large damping $\alpha \rightarrow \infty$ we have $A(\alpha S) \rightarrow 1$, and Eq. (9) reproduces the escape rate in the intermediate-to-high (IHD) damping range [37].

The dimensionless action S in the depopulation factor (13) is given in case of a magnetic particle by the integral ($p = \cos \theta$) [9,11]

$$S = \frac{V_p}{k_B T} \oint_{E=E_{\text{sad}}} \left[[1 - p^2(\phi)] \frac{\partial \epsilon}{\partial p} d\phi - \frac{1}{1 - p^2} \frac{\partial \epsilon}{\partial \phi} dp \right], \quad (14)$$

where ϵ denotes the energy density, expressed as the function of spherical coordinates of the magnetic moment: $\epsilon = \epsilon(\theta, \phi)$. This integral should be taken along the trajectory where the system energy E is equal to the saddle-point energy E_{sad} ; hence, the polar angle θ can be viewed as a function of the azimuthal angle ϕ , so that $p \equiv \cos \theta = p(\phi)$.

To evaluate the action (14), we shall use the energy density expression (2) and introduce the reduced energy density $u(m_y, m_z)$ as

$$u(m_y, m_z) = C_{yx} m_y^2(\theta, \phi) + C_{zx} m_z^2(\theta, \phi) \quad (15)$$

so that the action takes the form

$$\begin{aligned} S &= \frac{2\pi M_s^2 V_p}{k_B T} \oint_{E=E_{\text{sad}}} \left[(1 - p^2) \frac{\partial u}{\partial p} d\phi - \frac{1}{1 - p^2} \frac{\partial u}{\partial \phi} dp \right] \\ &= \frac{2\pi M_s^2 V_p}{k_B T} [I_1 + I_2]. \end{aligned} \quad (16)$$

$$I_1 + I_2 = -4C_{yx}\sqrt{\kappa} \int_0^\pi \left[\frac{\sin \phi}{(1 + \kappa \sin^2 \phi)^{1/2}} + \frac{\kappa \sin \phi \cos^2 \phi}{(1 + \kappa \sin^2 \phi)^{3/2}} \right] d\phi = -4C_{yx}\sqrt{\kappa}(1 + \kappa)I(\kappa) \quad (22)$$

(the minus sign appears due to the chosen integration direction along the trajectory and hence can be ignored, as we need only the absolute value of the action).

For $\kappa \geq 0$ the integral $I(\kappa)$ in (22) can be evaluated analytically: $I(\kappa) = 2/(1 + \kappa)$. Hence, the final result for the action S is

$$S = 16\pi \frac{M_s^2 V_p}{k_B T} \sqrt{C_{yx} C_{zy}}. \quad (23)$$

An important remark is in order. The depopulation factor A [Eq. (13)] depends on the product αS . Hence, it is clear already from the prefactor in the action expression (16) that the parameter which defines whether we are in the region of a small, intermediate, or large damping is *not* the value of the damping parameter α by itself, but the value of the *product* of

In the spherical coordinate system with the polar axis along the Cartesian x axis, and ϕ defined as the angle between the projection of \mathbf{m} onto the yz plane and y axis, we have $m_x = \cos \theta$, $m_y = \sin \theta \cos \phi$, $m_z = \sin \theta \sin \phi$, so that the energy density (15) is

$$\begin{aligned} u(\theta, \phi) &= \sin^2 \theta (C_{yx} \cos^2 \phi + C_{zx} \sin^2 \phi) \\ &= \sin^2 \theta C_{yx} (1 + \kappa \sin^2 \phi) \\ &= C_{yx} (1 - p^2) (1 + \kappa \sin^2 \phi), \end{aligned} \quad (17)$$

where the ratio $\kappa = (C_{zx} - C_{yx})/C_{yx} = C_{zy}/C_{yx} > 0$ is introduced.

The integration trajectory passes through the saddle point ($\theta = \pi/2$, $\phi = 0$) and hence the function $u(\theta, \phi)$ along this trajectory is equal to $u = u_{\text{sad}}(\pi/2, 0) = C_{yx}$, leading to the relation

$$(1 - p^2)(1 + \kappa \sin^2 \phi) = 1. \quad (18)$$

Using this condition by calculating partial derivatives of the energy density (17) and substituting them into the integral (16), we obtain

$$\begin{aligned} I_1 &= \oint_{u=u_{\text{sad}}} [1 - p^2(\phi)] \frac{\partial u}{\partial p} d\phi = -4C_{yx} \int_0^\pi p(\phi) d\phi, \quad (19) \\ I_2 &= - \oint_{E=E_{\text{sad}}} \frac{1}{1 - p^2} \frac{\partial u}{\partial \phi} dp = -C_{yx} \kappa \oint_{u=u_{\text{sad}}} \sin 2\phi \frac{dp}{d\phi} d\phi. \end{aligned} \quad (20)$$

Employing the same relation (18), we can find the derivative

$$\frac{dp}{d\phi} = \pm \sqrt{\kappa} \frac{\cos \phi u}{(1 + \kappa \sin^2 \phi)^{3/2}}, \quad (21)$$

where the upper sign corresponds to the interval $\phi \in [0, \pi]$, the lower sign to $\phi \in (\pi, 2\pi)$. Substituting this derivative into (20) and reducing integration limits over ϕ to $[0, \pi]$, we obtain

α and the relation of the energy barrier to the thermal energy $\Delta E/k_B T$ ($\sim M_s^2 V/k_B T$ in our case). We shall return to this statement below by comparing the results obtained by various methods.

III. LANGEVIN DYNAMICS (LD) SIMULATIONS

The most straightforward method to determine the switching rate between the two metastable system states is the simulation of the system dynamics in presence of thermal fluctuations using the corresponding stochastic equation of motion [38]. Taking into account that we are interested in magnetic systems by temperatures much lower than the Curie temperature (so that the magnetization magnitude

$M = \text{const}$), we use the Landau-Lifshitz-Gilbert equation

$$\begin{aligned} \frac{d\mathbf{M}}{dt} = & -\gamma[\mathbf{M} \times (\mathbf{H}_{\text{det}} + \mathbf{H}_{\text{fl}})] \\ & -\gamma \frac{\lambda}{M_s} [\mathbf{M} \times [\mathbf{M} \times (\mathbf{H}_{\text{det}} + \mathbf{H}_{\text{fl}})]] \end{aligned} \quad (24)$$

to describe the system dynamics. Here, the fluctuation field accounting for thermal fluctuations has the properties $\langle \mathbf{H}_{\zeta}^{\text{fl}} \rangle = 0$ and $\langle \mathbf{H}_{\zeta}^{\text{fl}}(0) \cdot \mathbf{H}_{\psi}^{\text{fl}}(t) \rangle = 2D_{\text{fl}}\delta(t)\delta_{\zeta\psi}$, where the fluctuation power is $D_{\text{fl}} = \lambda/(1 + \lambda^2)(k_B T/\gamma\mu)$ ($\zeta, \psi = x, y, z$), μ being the magnetic moment magnitude. The deterministic field \mathbf{H}_{det} contains the contributions from all magnetic energy terms, what in our case reduced to the anisotropy field only (we recall that we simulate nanoelements in the absence of an external field). The constant γ in (24) relates to the gyromagnetic ratio γ_0 and the damping α in the alternative form of this equation proposed by Gilbert $\dot{\mathbf{M}} = -\gamma_0[\mathbf{M} \times (\mathbf{H} - (\alpha/M_s)\dot{\mathbf{M}})]$ as $\gamma \approx \gamma_0$ via $\gamma = \gamma_0/(1 + \alpha^2)$, and damping parameters λ and α are equal; for further details, see, e.g., [39].

We have performed LD simulations using our micromagnetic package MICROMAGUS[40] where Eq. (24) is integrated using one of the adaptive step-size algorithms (Runge-Kutta or Bulirsch-Stoer) for the stochastic differential equations (SDE) describing the dynamics of vector fields with the constant vector magnitudes. The possibility to apply such methods to SDE (24) is justified in [41], where we have shown that for $M = \text{const}$ both Ito and Stratonovich stochastic calculi lead to identical results. For generation of the thermal noise we have used the version of the vector statistics (VS) Gaussian random numbers generator from Intel MKL library, which employs the inverse cumulative distribution function method (ICDF-type generator) to produce a sequence of independent Gaussian random numbers with the prescribed mean and distribution width; this generator is known for its high quality. Cross checks with other (simpler) random number generators, like those from [42], have shown that final results remain the same (in frames of statistical errors).

Simulation of magnetization switching using Langevin dynamics is possible only for systems with relatively small energy barriers (not higher than $\Delta E \sim 10 k_B T$) because simulation times grow exponentially with the energy barrier. For this reason we could perform LD studies only for macrospins corresponding to nanoellipses with $a = 50 \text{ nm}$ ($\Delta E \approx 9 k_B T$) and $a = 55 \text{ nm}$ ($\Delta E \approx 14 k_B T$); we remind that $T = 300 \text{ K}$.

Taking into account that both energy minima for our system are equivalent ($H_{\text{ext}} = 0$), the average switching time $\tau_{\text{sw}}^{\text{LD}}$ for LD simulations can be computed as

$$\tau_{\text{sw}}^{\text{LD}} = \frac{t_{\text{sim}}}{N_{\text{sw}}}, \quad (25)$$

where t_{sim} denotes the (physical) simulation time and N_{sw} the number of switching events between the energy minima observed during the simulation run.

However, in order to calculate $\tau_{\text{sw}}^{\text{LD}}$ properly, we have to correctly determine whether the true switching (defined as the transition between two metastable energy minima with $m_x = \pm 1$) took place. For this purpose, it is not enough to count the number of times when the dependence $m_x(t)$ changes its sign [see Fig. 4(a)] (or, to be more careful, crosses

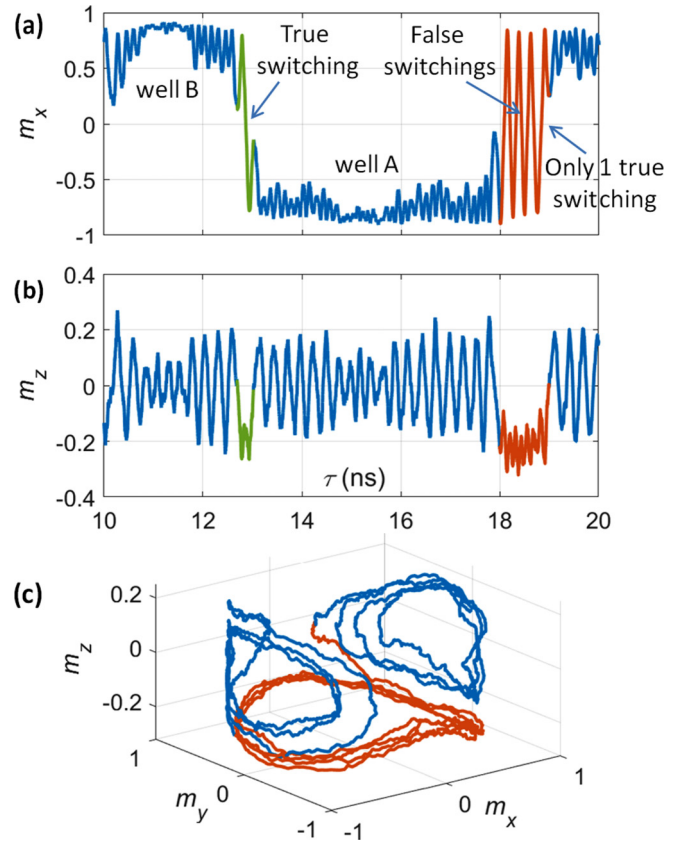


FIG. 4. Difference between “true” and “false” switchings (see text for details). On (c) the 3D magnetization trajectory in the time interval $17 \text{ ns} \leq \tau \leq 20 \text{ ns}$ is depicted.

some negative threshold, say, $m_x = -0.2$, when coming from positive values). For the correct determination of N_{sw} we have to distinguish between true and false switchings.

A simple example where this difference is clear is illustrated in Figs. 4(a)–4(c). Here, a true switching has occurred at $\tau \approx 13 \text{ ns}$; corresponding pieces on the dependencies $m_x(t)$ (which changes sign during the switching) and $m_z(t)$ are drawn in green. But, the (numerous!) sign changes of $m_x(t)$ in the interval $\tau \approx 18$ – 19 ns clearly do not correspond to any real switching process. 3D representation of the corresponding piece of the magnetization trajectory, marked in red in Fig. 4(c), demonstrates that these sign changes of m_x are due to the so-called out-of-plane (OOP) precession. By this precession kind the magnetization rotates in the high-energy region of the energy landscape (because $\|m_z\|$ is relatively large), so that during this process no real switching between the energy minima occurs. Hence, in Fig. 4 during the time interval $17 \leq \tau \leq 20 \text{ ns}$ only one real switching is observed.

To distinguish between true and false switchings, one could in principle perform the analysis of “candidate” cases, i.e., events when the sign change of m_x has been detected, using the time dependencies of other magnetization projections. For example, for the particular case shown in Fig. 4, the m_z projection does not change its sign during the whole time interval marked in red, indicating that the magnetization precession takes place only on one side of the easy plane of the nanoelement ($m_z \leq 0$), meaning that the OOP precession

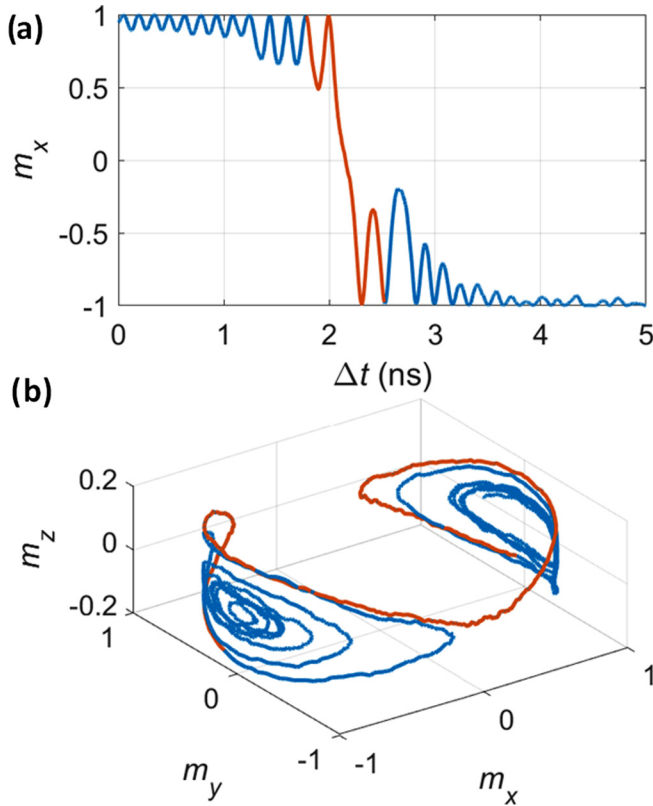


FIG. 5. Excitation of the macrospin before and its equilibration after the true switching as $m_x(t)$ dependence (a) and 3D magnetization trajectory (b) (the switching process itself is highlighted in dark red). Only the switchings after which the macrospin spends in the new basin more time than the equilibration time (≈ 3 ns) are counted as true switching events.

(and not a true switching) is in process. However, consideration of all particular cases would make the corresponding “projection-based” differentiating algorithm too complicated and thus unreliable.

For this reason, we have adopted a more general method to identify true switching events. The method is based on the very definition of “switching” which is understood as a transition between two metastable states, whereby the system under study must spend sufficient time in the vicinity of each state in order to achieve a partial thermal equilibrium within corresponding energy basins. If this is not the case, the switching is considered as false.

The idea is illustrated in Figs. 5 and 6. During a true switching (Fig. 5) the magnetic moment is first excited by thermal fluctuations so that it can overcome the energy barrier, and afterward the equilibration in the other energy well takes place. This equilibration, as shown in Fig. 5(a), takes about $t_{\text{eq}} \approx 2$ ns, whereby t_{eq} depends mainly on the damping parameter λ and slightly on the energy landscape near the energy minima. Based on this finding, we consider a switching as being “true” when the time Δt_{well} spent by the system in the target energy well after the switching is larger than t_{eq} .

To further support this idea, we have collected the histogram of time intervals between two subsequent sign changes of $m_x(t)$. This histogram shows a huge peak for small

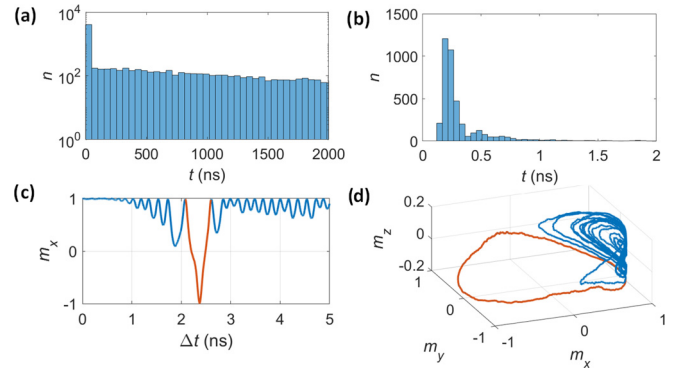


FIG. 6. (a) The region of the histogram of τ_{sw} obtained from LD simulations when *all* time moments when m_x changes sign are counted as switchings (note the log scale of the y axis). (b) The region of this histogram for $t < 1$ ns. (c) A typical $m_x(t)$ dependence for a false switching event [taken from the $\rho(\tau_{\text{sw}})$ peak shown in (b)] and (d) the corresponding 3D magnetization trajectory.

time intervals, as shown in Fig. 6(a) (note the logarithmic scale of the y axis!); this peak is presented in Fig. 6(b) in a much higher resolution. The analysis of magnetization trajectories corresponding to the events attributed to this peak has clearly demonstrated that these events typically represent an “excursion” of the magnetization toward the opposite energy minimum [see trajectories in Figs. 6(c) and 6(d)], and are clearly “false” switchings. So, in further analysis we have used the criterion $\Delta t_{\text{well}} > t_{\text{eq}}$ to identify real (true) switching events in LD simulations.

In order to obtain a sufficiently accurate statistics, for nanoelements with $a = 50$ nm, we have simulated a collection of 100 macrospins during $t_{\text{sim}} = 150 \mu\text{s}$ and for elements with $a = 55$ nm an ensemble of 400 macrospins during $t_{\text{sim}} = 5$ ms = 5×10^6 ns, applying the approach described in our paper [23]. After subtracting false switching events (using the criterion described above), we have obtained $\tau_{\text{sw}}^{\text{LD}}(a = 50 \text{ nm}) = 2.36(\pm 0.3) \times 10^3$ ns and $\tau_{\text{sw}}^{\text{LD}}(a = 55 \text{ nm}) = 1.3(\pm 0.2) \times 10^5$ ns. Note that for $a = 50$ nm the switching time is ≈ 1.6 times and for $a = 55$ nm about 1.4 times larger than the analytical values for these elements given by (9). This difference is most probably due to the fact that the approximation (9) does not take into “return” trajectories and thus overestimates the transition rate.

IV. TIME-TEMPERATURE EXTRAPOLATION METHOD (TTE)

The most straightforward idea which can be used to obtain switching rates for systems with energy barriers unachievable for standard LD simulations at room temperature is to perform LD simulations at higher temperatures and extrapolate obtained switching rates to the temperature of interest. From the quantitative point of view, this method (which we shall call the time-temperature extrapolation method or TTE) employs the assumption that the main temperature dependence of τ_{sw} is due to the exponential factor in the expression $\tau_{\text{sw}} = \tau_0 \exp(\Delta E/k_B T)$ and all other dependencies on T , which may be hidden in the prefactor τ_0 , are weak. This assumption implies that we can try to overcome the inherent limitation

of the Langevin dynamics' ability to model only systems with relatively low barriers in the following way.

For a system with a high-energy barrier we should perform LD simulations of the magnetization switching at several temperatures (all of them much larger than the temperature of interest), thus obtaining the dependence $\tau_{\text{sw}}(T)$ at relatively high temperatures. Then we can use the analytical form $\tau_{\text{sw}} = c \exp(b/T)$ to extrapolate the obtained dependence $\tau_{\text{sw}}(T)$ toward the desired low temperature (we note that a somewhat similar idea was used in [33] to obtain hysteresis loops in a low-frequency external field at a low temperature by simulating the loops in a high-frequency field at much larger temperatures).

The main physical deficiency of this idea is that by simulations at elevated temperatures the system will spend most of the simulated time in regions of the energy landscape which are inaccessible for this system at actual transition temperatures. However, as long as switching events remain relatively rare (so that the system mostly stays in the vicinity of energy minima), we can hope that the accuracy of the extrapolated result is reasonable.

The precision of the proposed method crucially depends on (i) the lowest temperature achievable in simulations for the given energy barrier and (ii) on the statistical accuracy of the switching time values (obtained in LD simulations) which will be used in the subsequent extrapolation. For our nanoelements, the lowest temperature for which LD simulations have been performed was chosen from the requirement that during the simulation time of 1 ms approximately 500 switching events should occur. Corresponding lowest temperature increases from $T_{\text{min}} = 600$ K for $a = 60$ nm to $T_{\text{min}} = 1800$ K for $a = 100$ nm. For two smallest elements $a = 50$ (55) nm we have stopped to decrease T at $T_{\text{min}} = 400$ (500) K in order to check how the extrapolation results agree with direct LD simulations available for $T = 300$ K for these nanoelements.

For each temperature, LD simulations were performed simultaneously for 100 nanoelements using our approach described in [23]. For each macrospin size a , averaged switching times obtained from these simulations $\tau_{\text{sw}}(T)$ were fitted using the function $\tau_a(T) = c_a \exp(b_a/T)$ where data points were weighted according to their statistical errors. An example of the corresponding fitting is shown in Fig. 7.

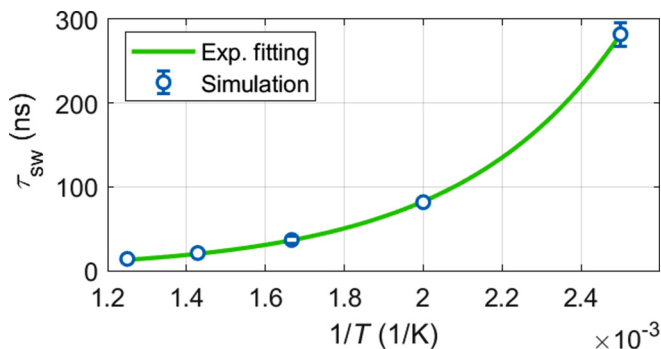


FIG. 7. Simulated temperature dependence of the switching time (open circles) and its fitting by the function $\tau = c_a e^{b_a/T}$ (solid line) for the macrospin corresponding to the nanoelement $a = 50$ nm.

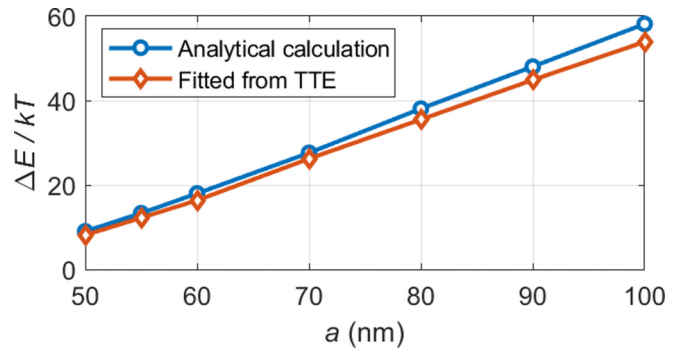


FIG. 8. Relation $\Delta E/k_B T$, obtained analytically using (6), compared with the coefficients b_a/T obtained from the fitting of TTE dependencies $\tau_a(T) = c_a \exp(b_a/T)$.

Interestingly, energy barrier $\Delta E^{\text{eff}}/k_B T = b_a/T$ obtained from this fitting was always somewhat smaller than the actual barrier $\Delta E/k_B T$ evaluated from the analytical expression (6), as shown in Fig. 8. As a consequence, for large barriers the switching time evaluated by the TTE method is smaller than the analytical result (9), as it will be discussed in Sec. VII

Finally, switching times for all sizes at room temperature were evaluated by extrapolating the fitting functions $\tau_a(T)$ to $T = 300$ K as shown in Fig. 9 by dashed green lines; switching times obtained this way are plotted in the same figure by red circles. Analysis of these results is postponed to Sec. VII,

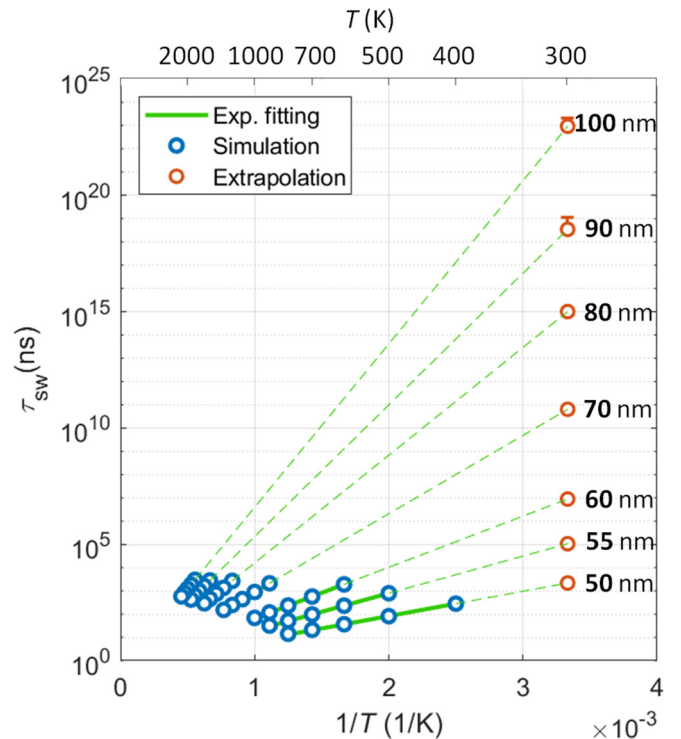


FIG. 9. Extrapolation of switching time obtained for higher temperatures using the LD dynamics (blue open circles) to $T = 300$ K (red open circles) for nanoelement sizes $a = 50$ –100 nm. The extrapolated τ_{sw} for the macrospin with $a = 50$ nm is $\tau_{\text{sw}}^{\text{TTE}} = 2.18(\pm 0.2) \times 10^3$ ns, for $a = 100$ nm it is $\tau_{\text{sw}}^{\text{TTE}} = 1.2(\pm 0.7) \times 10^{23}$ ns.

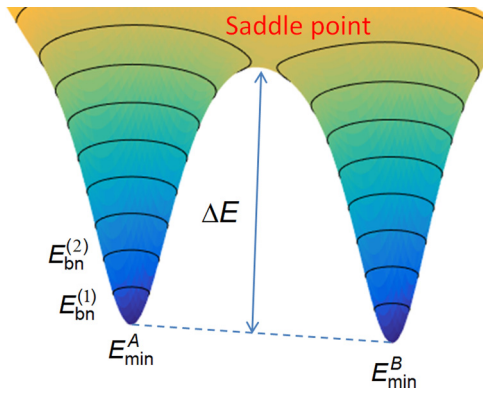


FIG. 10. Energy landscape with “bounce energy” contours E_{bn} .

where switching times obtained by all methods (analytical and numerical) will be compared.

V. ENERGY BOUNCE METHOD

A. Basic idea and analysis of the original methodology

The main idea of the “energy bounce” algorithm [30] is to enable LD simulations of the switching rate for arbitrary high-energy barriers by forcing the point representing the system state in the phase space to climb an “energy ladder” from the energy minimum to the saddle point. For this purpose, the energy interval ΔE between the minimum and the saddle is divided into much smaller intervals (in our simulations we have used $\delta E = k_B T$). Corresponding “splitting” of the energy landscape is visualized in Fig. 10.

Now, we start LD simulations from the energy minimum and continue until the energy histogram is computed with a sufficient accuracy (the importance of this criterion will be explained below). At the next stage, simulations start from some state (achieved so far) with the energy $E \geq E_{\min} + \delta E = E_{bn}^{(1)}$ and all LD steps which would lead to a state with an energy $E < E_{bn}^{(1)}$ are rejected, i.e., the system is allowed to move only in its phase-space region defined by the condition $E \geq E_{bn}^{(1)}$. Again, these LD simulations run until the accumulated energy histogram in this energy interval is sufficiently accurate (the duration of our LD simulations above each $E_{bn}^{(i)}$ is $t_{\text{walk}} = 2000$ ns). Then, at the next stage the minimal allowed energy is again increased by δE (i.e., LD steps are rejected if $E < E_{bn}^{(2)} = E_{bn}^{(1)} + \delta E$), etc.

This procedure is repeated until the bounce energy $E_{bn}^{(i)}$ is only a few $k_B T$ lower than the saddle point, so that a sufficient number of transitions over the saddle is observed by LD simulations above $E_{bn}^{(i)}$. In other words, for these values of $E_{bn}^{(i)}$ the apparent escape time from the energy well A (see Fig. 10) $\tau_{A,\text{app}}^{(i)} = \Delta t_A^{(i)} / N_{\text{sw}}^{(i)}$ can be computed with a reasonable precision (here $\Delta t_A^{(i)}$ is the time spent in the well A during LD simulations with $E > E_{bn}^{(i)}$).

The key question here is how to connect the time $\Delta t_A^{(i)}$ spent by the system within A for trajectory obeying the condition $E > E_{bn}^{(i)}$, with the time spent in this well for unconstrained simulations. As the energy near the saddle can not be achieved for unconstrained simulations within a reasonable time, this connection can be established only recursively, i.e.,

the time $\Delta t_A^{(i)}$ spent in A during simulations with $E > E_{bn}^{(i)}$ should be related to $\Delta t_A^{(i-1)}$ during the previous stage (when $E > E_{bn}^{(i-1)}$). If we denote the corresponding proportionality coefficient as F_i , i.e., $\Delta t_A^{(i)} = F_i \Delta t_A^{(i+1)}$, then for the determination of the actual switching rate we obtain the expression

$$\Gamma_n^{\text{EnB}} = \prod_{j=1}^{n-1} F_j \frac{N_{\text{sw}}^{(n)}}{\Delta t_A^{(n)}}, \quad (26)$$

where n is the total number of bounce energy levels used to climb the path from the energy minimum to the saddle point.

Before proceeding to the detailed consideration of methods for the computation of F_i , we emphasize that these coefficients have to be determined with a very high precision, whereby systematic errors are especially dangerous. This feature follows directly from the basic expression (26), which involves the *product* of all F_i , meaning that any systematic error by their calculation will be exponentially amplified.

In the original version [30] it was suggested to determine F_i from the probability densities $\rho_i(E | E > E_{bn}^i) \equiv \rho_i(E)$ to encounter the energy E at the i th stage. Namely, in [30] it was assumed that the probability density $\rho_{i+1}(E)$ is simply proportional to the corresponding probability density $\rho_i(E)$. This would mean that $\rho_i(E) = F_i \rho_{i+1}(E)$, where the “transfer coefficient” F_i does not depend on E (for $E > E_{bn}^{(i)}$, i.e., if the energy E is accessible for both stages i and $i+1$). This independence of F_i on E is the main assumptions in this version of the energy bounce method. It can be verified only by the direct comparison of energy histograms obtained at stages i and $i+1$.

According to [30], the proportionality $\rho_i(E) = F_i \rho_{i+1}(E)$ approximately holds except for the energies close to $E_{bn}^{(i+1)}$. Basing on this finding, and in order to increase the accuracy by the calculation of F_i , Wang and Visscher [30] have suggested to compute F_i using the integral ratio

$$F_i^{(\text{int})} = \frac{\int_{E_{bn}^{(i+1)} + \epsilon_{\text{off}}}^{\infty} \rho_i(E) dE}{\int_{E_{bn}^{(i+1)} + \epsilon_{\text{off}}}^{\infty} \rho_{i+1}(E) dE}, \quad (27)$$

where the lower limit of both integrals is larger than $E_{bn}^{(i+1)}$ by an offset energy ϵ_{off} ($= k_B T$ in [30]) to exclude the above-mentioned histogram region near $E_{bn}^{(i+1)}$.

Analyzing the energy histograms from our simulations, we could confirm that the ratio $\rho_i(E) / \rho_{i+1}(E)$ is approximately constant, except for the regions near the bounce energies, where this ratio becomes singular [as shown in Fig. 12(b)] because $\rho_{i+1}(E) \rightarrow 0$ for $E \rightarrow E_{bn}^{(i+1)}$ (see Fig. 11). This feature of accumulated histograms shows that the true thermodynamic equilibrium is not achieved near the bounce energies [we note that the density of state $D(E)$ has no zeros or singularities near $E_{bn}^{(i)}$]. In [30] it was suggested that this is due to the finite size of the LD time step. Indeed, our studies have shown that the width of the disturbed area [where the accumulated energy histogram strongly differs from the true-equilibrium result, see Fig. 11(b)] decreases when the LD step size becomes smaller. However, this decrease is very slow so that for any reasonable time

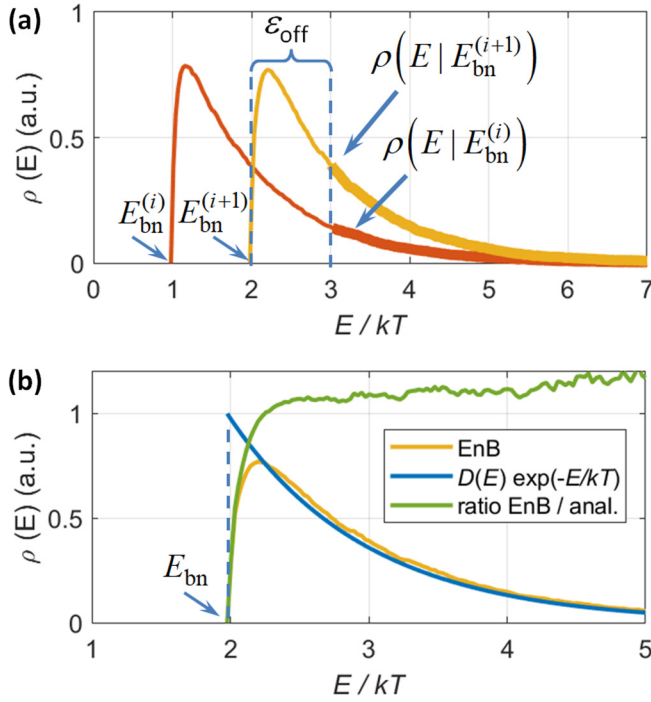


FIG. 11. (a) Energy histograms sampled at two subsequent values of the bounce energy. The offset ϵ_{off} marks the regions above $E_{\text{bn}}^{(i+1)}$ where the histogram does not correspond to the thermodynamic equilibrium due to the influence of the “hard” energy cutoff at E_{bn} . (b) Energy histogram sampled by simulations (yellow line) compared to the exact analytical result (4) for the probability to obtain the energy E in a true equilibrium (blue line); the ratio of the simulated histogram to the analytical result is shown by the green line.

step the width of the out-of-equilibrium energy interval remains substantial. To avoid this region, we have also used the offset energy $\epsilon_{\text{off}} = k_B T$ (Fig. 11). Consequences of the existence of this disturbed region for the switching rate computed via the expression (26) will be discussed in Sec. VII.

In addition to the problem discussed in the previous paragraph, the ratio $\rho_i(E)/\rho_{i+1}(E)$ exhibits a small systematic decrease when the energy increases [see Fig. 12(b)]. To study whether this systematic decrease affects the computed switching time, we have tested another method for the evaluation of F_i , based as average ratio of histograms

$$F_i^{(\text{av})} = \left\langle \frac{\rho_i(E)}{\rho_{i+1}(E)} \right\rangle_{E_{\text{bn}}^{i+1} + \epsilon_{\text{off}} < E < E_{\text{max}}^{i+1}} \quad (28)$$

computed at the interval from the offset energy to the maximal energy E_{max}^{i+1} for which $\rho_{i+1}(E)$ becomes too small (typically less than 5% of its maximal value) so that the ratio $\rho_i(E)/\rho_{i+1}(E)$ becomes ill defined due to statistical fluctuations of accumulated histograms. The product of F_i (see Fig. 13) and switching times (shown in Fig. 17 for two different macrospin sizes) were very close to those obtained using the initial definition (27), showing the high robustness of both methods for evaluating F_i for a macrospin.

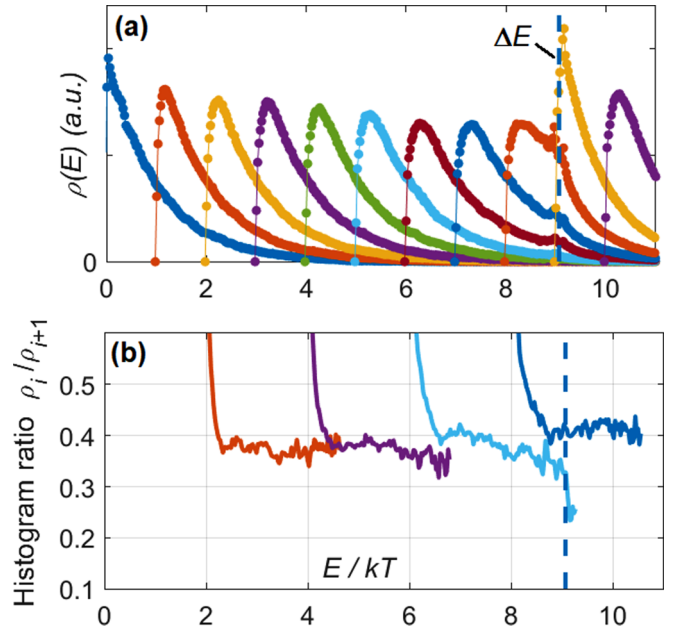


FIG. 12. (a) Energy histograms $\rho_i(E)$ for subsequent stages of the energy bounce method ($\delta E = k_B T$); (b) ratios $\rho_{i+1}(E)/\rho_i(E)$ for some histogram pairs (for the macrospin with $a = 50$ nm).

B. Alternative method to define transition coefficients

Unfortunately, the energy bounce algorithm based on the evaluation of transfer coefficients F_i employing energy histograms (not to mention the assumption of their proportionality) cannot be used for full-scale micromagnetic simulations, where other energy contributions, in addition to the shape anisotropy energy present for a macrospin, play an important role. The major problem is that the height of an energy barrier in typical magnetic systems is determined by either the magnetocrystalline anisotropy E_{an} or the magnetodipolar energy E_{dip} (which is responsible for the shape anisotropy introduced *ad hoc* in the macrospin approach), whereby the energy itself is largely determined by the exchange stiffness energy E_{exch} . The latter contribution is especially high by simulations including thermal fluctuations

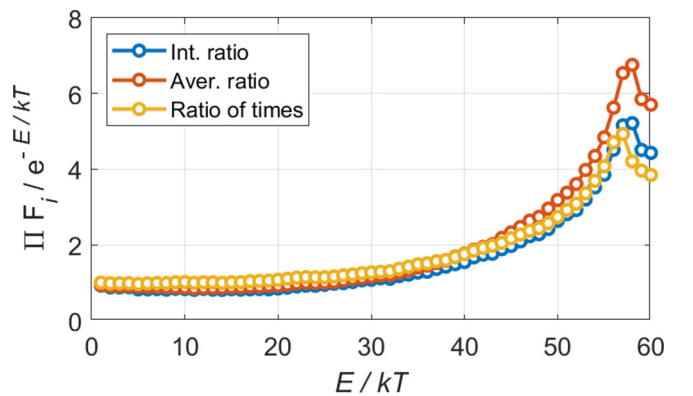


FIG. 13. (a) Product of coefficients F_i as the function of the bounce energy for various methods to evaluate F_i . (b) Ratios of the products $F_i^{(\text{int})}$ and $F_i^{(\text{av})}$ to the product of $F_i^{\Delta t}$ (for the macrospin with $a = 100$ nm).

(what is mandatory for studies of thermally activated switching), and may exceed both E_{an} and E_{dip} by several orders of magnitude.

This feature of E_{exch} makes the usage of histograms of the total energy completely impractical because the energy of interest, e.g., E_{dip} in case of shape-anisotropic particles, would represent only a tiny contribution to this (noisy!) histogram. Further, the analysis of histograms of E_{dip} only would also be not really helpful because in a strongly interacting system no general statements concerning the statistical distribution of some part of the total energy (like the existence of the Boltzmann distribution) can be made, not to mention some proportionality assumptions like those used in [30].

For this reason, we suggest to use a qualitatively different method to compute the coefficients F_i , which employs our definition of F_i as proportionality coefficients between the time interval $\Delta t_A^{(i+1)}$ spent in **A** during simulations with $E > E_{\text{bn}}^{(i+1)}$ and the corresponding interval $\Delta t_A^{(i)}$ during the i th stage (when $E > E_{\text{bn}}^{(i)}$), i.e.,

$$F_i^{(\Delta t)} = \frac{\Delta t_A(E > E_{\text{bn}}^{i+1} + \epsilon_{\text{off}})}{\Delta t_A(E > E_{\text{bn}}^i + \epsilon_{\text{off}})}. \quad (29)$$

Results of simulations where this definition of F_i has been used turned out to be in a very good agreement with the original method (27) and its modification (28) for all macrospin sizes studied in this paper, as shown in Fig. 13 on an example for $a = 100$ nm.

The advantages of this method are twofold: (i) it is very simple and much faster than histogram-based methods because one does not need to accumulate energy histograms with the high accuracy required for the precise determination of F_i , and (ii) it can be applied to systems, where only one contribution to the total energy should be monitored, no matter what the distribution of this energy term looks like. Using a slightly modified definition (29) of F_i , we could expand the energy bounce method toward full-scale micromagnetic simulations using the magnetodipolar energy of the spatially averaged nanoelement magnetization as the energy of interest entering (29). Corresponding results, being out of scope of this publication, will be reported elsewhere.

Next, the problem how to determine another key quantity in (26), the number of “true” switchings $N_{\text{sw}}^{(n)}$ over the barrier when the system stays above the bounce energy level $E_{\text{bn}}^{(n)}$, should be considered. The method described in Sec. III which is based on the criterion $\Delta t_{\text{well}} > t_{\text{eq}}$ is not applicable here because no real thermal equilibration occurs after switching due to the artificial restriction imposed on the system energy ($E \geq E_{\text{bn}}^{(n)}$).

For this reason, we have decided to consider a switching as being “true” if after changing sign of m_x , the system completes at least one precession cycle around the new equilibrium orientation of the magnetic moment.

This criterion was supported again by the analysis of histograms of time intervals between subsequent sign changes of m_x , which always look like the example shown in Fig. 14: a large peak at very small time intervals followed by smaller but well-distinguished peaks for larger Δt 's. The visualization of magnetization trajectories corresponding to these peaks has shown that the first peak corresponds entirely to magne-

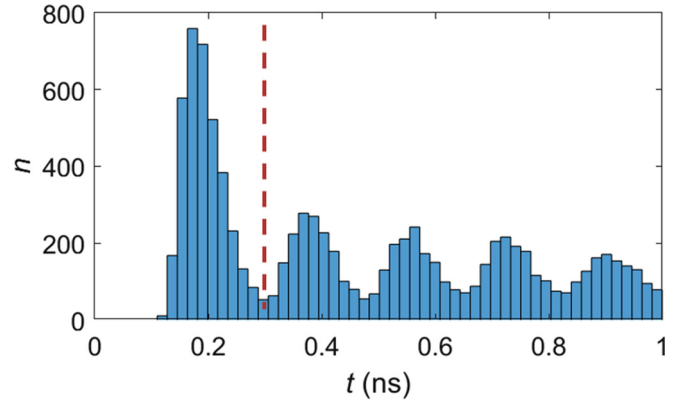


FIG. 14. Histogram of switching times for the macrospin with $a = 70$ nm for the bounce energy near the energy barrier ($E_{\text{bn}} = \Delta E - 5kT$). The first peak corresponds to the out-of-plane precession cycles [see Figs. 15(a) and 15(b)], so that these events are not counted as switchings

tization “excursions” toward the opposite energy minimum, where in most cases one cycle of the OOP precession is accomplished [see Figs. 14(a) and 14(b)]. The next peaks contained real switching events, where the number of precession cycles around the energy minimum was equal to the sequence number of corresponding peak in the histogram (if the first peak is not counted) [see an example in Figs. 14(c) and 14(d)]. For these reasons, the switching was considered as being true, if the time spent in the energy basin after switching exceeded the time separating the OOP peak and the next peak on the histogram $\rho(\Delta t_{\text{well}})$; the corresponding threshold is shown in Fig. 14 by the red dashed line.

The remaining question is how to choose the total number of energy bounce levels n which is best suited for the switching rate computation. This question is briefly addressed in [30], but a more detailed discussion is clearly necessary. Namely, the stability of the evaluation of Γ^{EnB} using (26) assumes the existence of a delicate balance between the product of F_i 's and the number of switching events $N_{\text{sw}}^{(n)}$ observed during LD simulations above the bounce energy $E_{\text{bn}}^{(n)}$. Whereas the product of F_i 's exponentially decreases with n , because $F_i < 1$ according to its definition (see Fig. 13), the number of switchings $N_{\text{sw}}^{(n)}$ should exponentially increase with n because we approach the saddle point. From the analytical point of view, these two tendencies should exactly compensate each other, providing the same answer for Γ^{EnB} no matter how many bounce levels we use.

However, in real simulations with the limited t_{walk} for each $E_{\text{bn}}^{(i)}$ a sufficiently large number of switchings ($N_{\text{sw}} > 100$) necessary to establish the exponential trend $N_{\text{sw}}^{(n)} \propto \exp(n)$ with a sufficient accuracy (Fig. 16) is observed only for high bounce energies $E_{\text{bn}}^{(i)} \geq \Delta E - 5kT$. On the other hand, the i th bounce energy level should not be too close to the energy barrier because otherwise the very concept of switching as a rare transition over the barrier becomes invalid. These two conditions leave a relatively narrow window of bounce energies where we really have $N_{\text{sw}}^{(n)} \propto \exp(n)$, as demonstrated in Fig. 16. Only in this interval of E_{bn} the switching time $\tau_{\text{sw}}^{\text{EnB}} = 1/\Gamma_n^{\text{EnB}}$ [see (26)] is approximately independent on

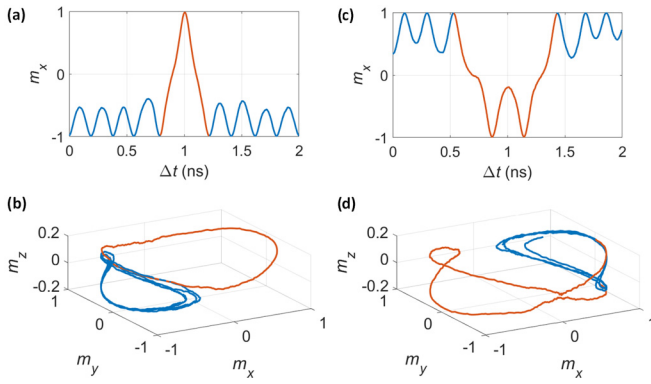


FIG. 15. Typical $m_x(t)$ dependencies and 3D magnetization trajectories for false (a), (b) and true (c), (d) switchings when E_{bn} is close to the energy barrier. Events shown on (a) and (b) correspond to the first peak and on (c) and (d) to the second peak on the histogram shown in Fig. 14.

the number of the bounce level n (see two examples in Fig. 17, where the plateaus suitable for the determination of τ_{sw} are explicitly marked). These plateaus should be determined manually, making the application of the whole method rather nontrivial.

Further, in order to improve the statistics in determination of $N_{sw}^{(n)}$, we have set $t_{walk} = 500$ ns for $E_{bn} < \Delta E - 5k_B T$, and increased t_{walk} to 10^5 ns for $E_{bn} \geq \Delta E - 5k_B T$. At the same time, the bounce energy step in this interval was decreased to $\delta E = 0.5k_B T$.

Comparison between switching times obtained using different versions (27)–(29) for the evaluation of transfer coefficients is given in Fig. 18. Overall, the agreement between all three versions can be considered as being fairly good: we emphasize here that computed switching times cover more than 20 orders of magnitude, so that they had to be divided by the exponential factor $\exp(\Delta E/k_B T)$ to enable a meaningful comparison between them on a single plot. Among all versions, our method (28) provides the best agreement with the results of LD simulations available for small barriers. Switching times computed according to the more universal method (29) (yellow curve) lie systematically somewhat lower than for other two versions (compare to Fig. 13). However, this difference becomes smaller than statistical errors when the energy barrier increases (for $\Delta E/k_B T \geq 30$),

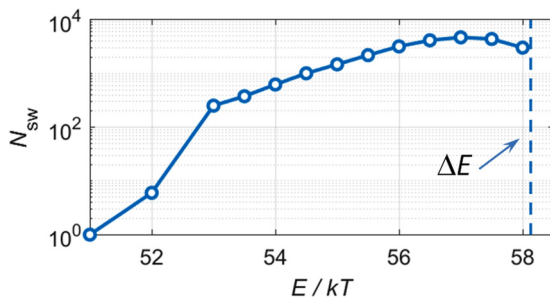


FIG. 16. Number of switchings as the function of the bounce energy for the macrospin with the long axis $a = 100$ nm.

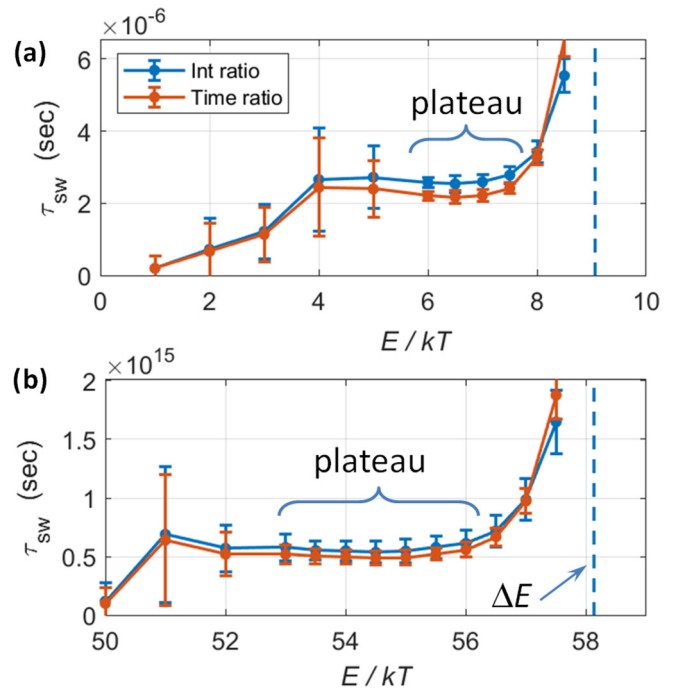


FIG. 17. Switching times as functions of the last bounce energy $E_{bn}^{(n)}$ for the macrospin with $a = 50$ nm (a) and with $a = 100$ nm (b) used for calculation of τ_{sw} via (26). Different line colors correspond to two approaches (27) and (29) for calculating F_i . Plateau which can be used to establish τ_{sw} are marked with curly brackets. Dashed lines show the energy barriers ΔE .

i.e., this energy bounce version is clearly applicable for the most interesting region of energy barriers.

The relation between switching times obtained with the energy bounce method and other methods (analytical and numerical) for all macrospin sizes studied here will be discussed in Sec. VII.

VI. FORWARD-FLUX SAMPLING (FFS)

The forward-flux sampling method was initially suggested as a method to evaluate switching rates between different

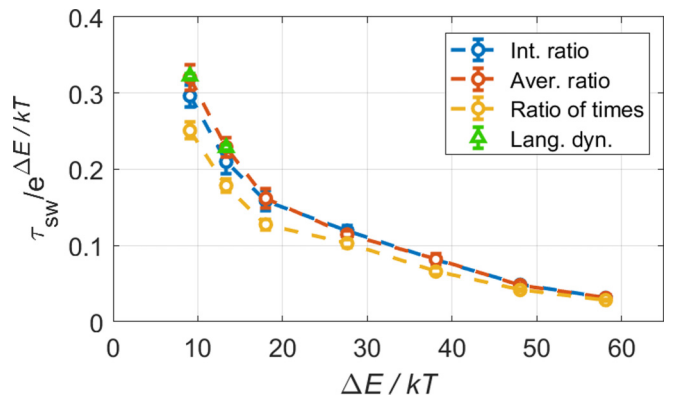


FIG. 18. Average switching time [divided by $\exp(\Delta E/k_B T)$ for the presentation clarity] obtained from the three approaches (27)–(29) used to compute τ_{sw} in the energy bounce method as the function of the energy barrier.

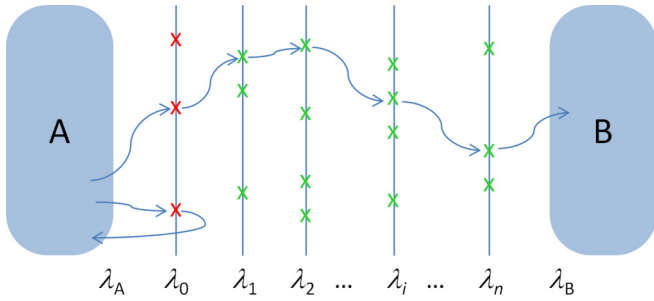


FIG. 19. Illustration of FFS method. Transition between wells **A** and **B** over interfaces λ_i .

metastable configurations of complex molecules in biochemistry [24]. In principle, FFS can be adopted to any biological, chemical, or physical applications where transition rates over high-energy barriers have to be evaluated, including micro-magnetic problems (see, e.g., [29]).

A. General methodology of FFS

The idea of FFS can be understood from Fig. 19. Basins **A** and **B** (in the corresponding system coordinate space) surrounding the two corresponding metastable states of interest are confined by the interfaces λ_A and λ_B . Intermediate interfaces λ_i , $i = 1, \dots, n$, are constructed in-between λ_A and λ_B so that transitions between two the subsequent interfaces i and $i + 1$ can be expected during LD simulations of the system within a reasonable time.

LD simulations are then started from the state $m_x = +1$ and thermalization within the basin **A** is carried out (i.e., simulations are performed until the average energy does not exhibit any systematic trend). Afterward, the flux per unit time out of the basin **A** is computed as the relation

$$\Phi_A = N_{A \rightarrow 0} / \Delta t_A, \quad (30)$$

where $N_{A \rightarrow 0}$ is the number of times when the system trajectory coming from the basin **A** has reached (crossed) the interface λ_0 during the simulation time interval Δt_A . System states corresponding to these N_0 crossings are saved as potential starting states for the next stage.

Next, M_0 trial trajectories are started from the states chosen randomly out of the set of above-mentioned N_0 saved states on the interface λ_0 . If a trial trajectory returns into the basin **A**, it is disregarded. If such a trajectory reaches the interface λ_1 , the system state corresponding to this crossing point is saved. If the total number of these crossing events is N_1 , then the conditional probability that a trajectory starting from the interface λ_0 will reach the interface λ_1 is $p(\lambda_1 | \lambda_0) = N_1 / M_0$.

Repeating the same procedure starting from the subsequent interfaces, we can then compute the required transition rate straightforwardly as

$$\Gamma^{\text{FFS}} = \Phi_A p(\lambda_B | \lambda_0) = \Phi_A \prod_{i=0}^n p(\lambda_{i+1} | \lambda_i), \quad (31)$$

where $\lambda_{n+1} = \lambda_B$; here, we have used the chain rule stating that the conditional probability $p(\lambda_B | \lambda_0)$ equals to product of corresponding conditional probabilities that a trajectory will reach the interface λ_{i+1} when having started from the

interface λ_i [$p(\lambda_{i+1} | \lambda_i) = N_{i+1} / M_i$]. In our simulations which results are presented below, we have used $N_{\text{att}} = 500$ attempts for each macrospin size and $M_i = 500$ trial trajectories for starting from each interface within the given attempt.

B. Positioning the interfaces based on the energy considerations

The FFS method as such does not contain any adjustable parameters like, e.g., the offset energy in the energy bounce method. The procedure described above leads to the unbiased estimation (31) of the escape rate. Hence, the primary question is how to maximize the efficiency of FFS, meaning how to minimize the statistical error of the computed escape rate for the fixed amount of the computer time spent by calculations.

This problem has been analyzed in details in several publications [26,27] treating FFS in general, i.e., without a reference to any specific physical system. This analysis has led to the intuitively expected result that the best efficiency of FFS is achieved when the flux between the two subsequent interfaces $M_i p(\lambda_{i+1} | \lambda_i)$ is constant “along” the system, in other words, does not depend on the interface number. Taking into account that the number of trial “shots” from each interface is usually the same, we arrive at the statement that in order to minimize the statistical error, we should construct the set of interfaces so that the transition probability $p_i \equiv p(\lambda_{i+1} | \lambda_i) = \text{const}$.

Several methods for the construction of the corresponding set $\{\lambda_i\}$ have been suggested [26,27]. All these methods are iterative and provide some recipes how to shift the interfaces $\{\lambda_i\}$ based on the transition probabilities p_i obtained on this set.

In our case, a much simpler solution is possible. We consider the escape of a physical system over an energy barrier, and thus have at our disposal the Boltzmann distribution $p \propto \exp(-E/k_B T)$ of the probabilities to find a system with an energy E at the temperature T . Hence, we can position the interfaces employing the idea that the transition probability between the two subsequent interfaces is roughly proportional to the energy difference between them: $p_i \propto \exp[(E_{i+1} - E_i)/k_B T]$. This relation is not exact, as there can be small deviations due to the dependence of the density of system states on the system energy, but this correction is usually small compared to the exponential dependence of the probability on the energy difference.

Using this proportionality, we introduce for the “uphill” path the set of interfaces, which are equidistant in the *energy space*. Namely, we first define the boundary λ_A of the basin **A** (from which we start the simulation) by the energy $E(\lambda_A) = E_{\min} + k_B T$. Then we place the interface λ_0 used for the flux calculation (30) one $k_B T$ higher: $E(\lambda_0) = E(\lambda_A) + k_B T$. Finally, we place the uphill interfaces λ_i ($i = 1, \dots, n$) so that $E^{\text{up}}(\lambda_i) \equiv E_i^{\text{up}} = E(\lambda_0) + i \delta E_{\text{if}}$, where the number of interfaces n is chosen so that (i) the last uphill interface is placed in the vicinity of the saddle point, but slightly beyond it, so that $E_n^{\text{up}} \approx E^{\text{sad}} = E_{\min} + \Delta E$, whereas $m_x(\lambda_n) < 0$ and (ii) the energy difference between the interfaces $\delta E_{\text{if}} \approx k_B T$.

The positioning of interfaces on the downhill path is less important because the flux toward the basin **B** after passing the saddle point is large, so that corresponding conditional probabilities rapidly tend to 1.0. Hence, we use here only two

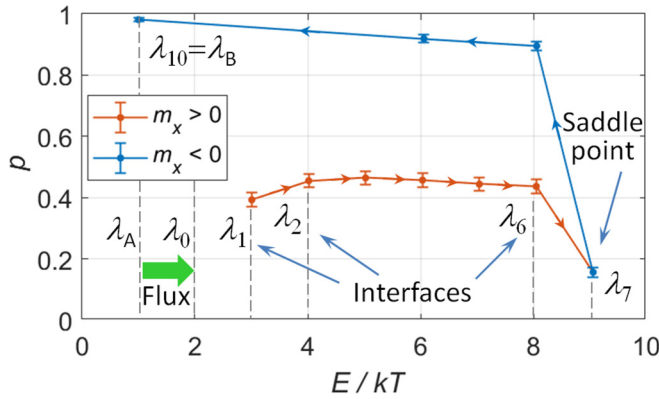


FIG. 20. Conditional probability p as the function of the interface energy E for the macrospin with $a = 50$ nm (energy barrier $\Delta E \approx 9k_B T$), obtained for 500 attempts and $N_i = 500$ starting points from each interface

additional interfaces with the energies $E_1^{\text{down}} = E^{\text{sad}} - k_B T$ and $E_2^{\text{down}} = E^{\text{sad}} - 3k_B T$.

Placing of interfaces in the energy space requires a special discussion because usually the interfaces are positioning in the coordinate space $\{\mathbf{x}\}$ of the studied system. From the mathematical point of view, assignment of interfaces in the energy space can be considered as a specific form of placing coordinate-based interfaces with coordinates defined via an implicit function $E_{\text{if}} = E_{\text{if}}(\mathbf{x})$. In our specific case where the energy is given by the simple expression (1), this implicit function, together with the relation $\|\mathbf{m}\| = 1$, defines closed ellipselike contours $C_{yx}m_y^2 + C_{zx}m_z^2 = E_{\text{if}}/2\pi m_s^2 V$, $m_x = \pm(1 - m_y^2 - m_z^2)^{1/2}$ on the unit sphere. The plus (minus) signs before the m_x projection correspond to interfaces on the uphill (downhill) path. In case of more complicated systems, e.g., in full-scale micromagnetic simulations, the simple recipe of placing interfaces using the total energy does not work for the same reason as the usage of this total energy as energy bounce intervals (see discussion in the Sec. VB). Corresponding extension of the interface positioning method will be discussed in the upcoming publication.

Using our methodology for the interface positioning, we have introduced another optimization which strongly reduces the total computation time. In the standard FFS version, the trajectory is abandoned (the attempt is considered as failed), when after having started from some interface λ_i , it returns to the initial basin A. We abandon a trajectory already when the corresponding energy drops below $E(\lambda_i) - 5k_B T$ because in this case it is exponentially unlikely that this trajectory ever climbs above the interface λ_i . For the highest-energy barrier studied here ($\Delta E \approx 60k_B T$), this optimization leads to $\approx 4\times$ acceleration of simulations.

An example for the dependence of the transition probability p_i between the interfaces on the interface number i (in fact, on the interface energy E_i) is shown in Fig. 20. It can be seen that for the uphill interfaces this probability is indeed nearly independent on E_i , thus ensuring the smallest possible statistical error by calculating the switching rate.

Switching times calculated using the FFS modified as described above are presented in Fig. 21 and will be discussed in the next section.

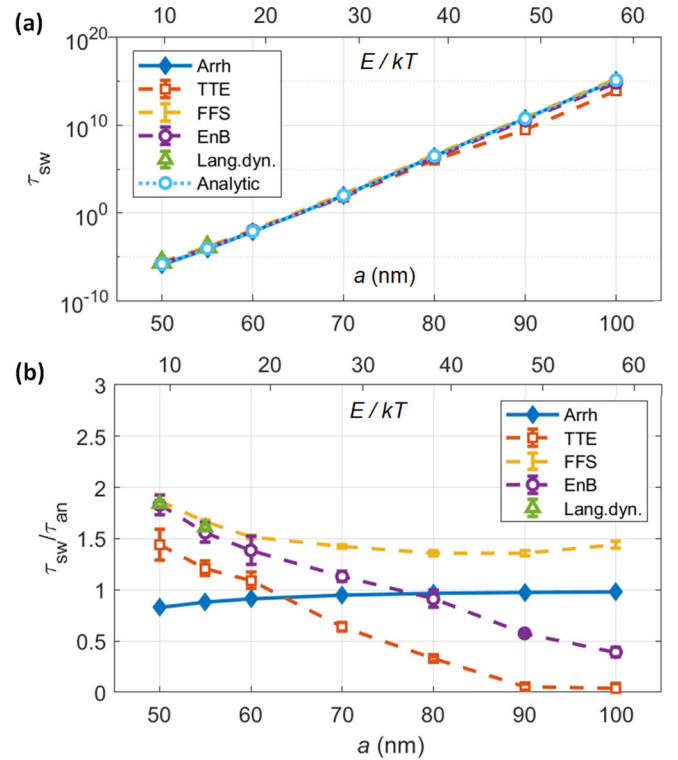


FIG. 21. Switching times in dependence on the macrospin size computed by all analytical and numerical methods (a) and ratio of switching times for all methods to the switching time obtained in the analytical approximation (9).

VII. RESULTS AND DISCUSSION: COMPARISON OF ANALYTICAL AND NUMERICAL METHODS

Results for the switching time dependencies on the macrospin size (long ellipse axis a) obtained with all analytical and numerical methods presented in this paper are collected in Fig. 21. First, we point out that in the interval of energy barriers $9 < \Delta E/k_B T < 70$ studied here, switching times span the interval of more than 20 orders of magnitude (from $\approx 2 \mu\text{s}$ to ≈ 30 million years). For all methods τ_{sw} grows (at least approximately) proportional to the relation $\Delta E/k_B T$, so that the difference between τ_{sw} measured by various methods is barely visible when τ_{sw} is plotted as the function of size [Fig. 21(a), logarithmic scale].

For this reason, in Fig. 21(b) we have plotted the ratio $\tau_{\text{sw}}/\tau_{\text{sw}}^{\text{an}}$ of switching time obtained by different methods to the corresponding time calculated using the analytical approximation (9), which is valid for $\Delta E \gg k_B T$ and should be applicable for arbitrary damping. This way we eliminate the exponential dependence of τ_{sw} on the energy barrier (or, equivalently, on the long axis a), enabling the meaningful comparison of various approaches.

First of all, we note a remarkable coincidence of the Arrhenius approximations (5)–(8) with the more general analytical result (9) in the whole range of switching times: $\tau_{\text{sw}}^{\text{Arr}}/\tau_{\text{sw}}^{\text{an}} \approx 1$ [see the blue line in Fig. 21(b)]. This agreement is due to the fact that for our system the product of damping $\alpha = 0.01$ and the ratio $10 < \Delta E/k_B T < 60$ lies in the range $0.1 < \alpha \Delta E/k_B T < 0.6$. As stated in Sec. II C, it is this product (and

not the damping value α by itself) which governs the transition between various damping regimes. Hence, the values of the parameter which controls the transition from the low to the high damping regime lie for our macrospins in the intermediate region, where a good agreement between the simple transition state theory (Arrhenius law) and the sophisticated analytical result (9) is indeed expected (see, e.g., Fig. 9 in [9]).

Next, we discuss the relation between switching times obtained by different numerical methods and the analytical approximation (9).

For relatively small energy barriers ($\Delta E/k_B T \leq 15$), where a comparison with straightforward LD simulations is still possible, all numerical methods agree with LD results within the statistical errors of the latter (only the TTE result is slightly below the LD value). Further, all numerically computed switching times for these small barriers are larger than the analytical ones ($\tau_{sw}^{num}/\tau_{sw}^{an} > 1$ for $a \leq 55$ nm, see Fig. 21). This relation is in accordance with the well-known feature of analytical approximations: they overestimate the transition rate (thus underestimating the switching time) because they do not take into account the possibility that a system trajectory can return to the initial basin A shortly after crossing the saddle (i.e., without visiting the basin B) [9]. Note that these “back-hopping” events should not be mixed up with the out-of-plane precession analyzed in Sec. III.

When the energy barrier increases, results of numerical methods exhibit considerably different trends.

Time-temperature extrapolation method. Relation of switching times obtained via TTE to analytically computed times decreases with increasing ΔE , becomes smaller than 1.0 for $\Delta E/k_B T \geq 20$, and drops to $\tau_{sw}^{TTE}/\tau_{sw}^{an} \approx 0.1$ for the largest particles studied here with $a = 90$ and 100 nm ($\Delta E/k_B T > 50$).

From the “technical” point of view, this decrease is due to the fact that “effective” energy barriers obtained by the exponential fitting of TTE switching times (computed by higher temperatures) are systematically lower than actual barriers, and this difference increases with the barrier height, as shown in Fig. 8. The most probable physical explanation of this behavior is that for larger energy barrier LD simulations in the TTE method have to be conducted by higher temperatures, so that magnetic moments precess in the higher-energy range than by the room temperature. In this energy range the curvature of the energy landscape (i.e., the density of states) is considerably different from the curvature near the bottom of the energy minimum, which may result in a lower “effective” energy barrier.

Still, we point out that this conceptually very simple (so that it can be easily extended to full-scale micromagnetics) and relatively fast method performs surprisingly well: In the interval of τ_{sw} covering more than 20 orders of magnitude, TTE switching times τ_{sw}^{TTE} differ in the worst case only by one order of magnitude from results obtained by much more sophisticated methods.

Energy bounce method. For this method, relation of its switching times to the analytical ones also decreases with the energy barrier, although much slower than for TTE. Still, the ratio $\tau_{sw}^{EnB}/\tau_{sw}^{an}$ drops below unity for $\Delta E/k_B T \geq 30$ and achieves the value ≈ 0.5 for $a = 100$ nm ($\Delta E/k_B T \approx 60$). Taking into account that the switching time computed

numerically should be larger than τ_{sw}^{an} (see the explanation above), the reason for this systematic decrease of the ratio $\tau_{sw}^{EnB}/\tau_{sw}^{an}$ should be found.

In the energy bounce expression for the switching rate (26), the number of switching events $N_{sw}^{(n)}$ at the n th stage of the method is determined using the same criteria as for the straightforward LD simulations without the bounce energy. Hence, the only possible source of the systematic underestimation of the actual switching time in the energy bounce algorithm is the systematic error by the computation of the transition factors F_i .

To explain the appearance of such deviation by computing F_i , we remind that these factors are evaluated using either the ratio of energy histograms obtained for different bounce energy levels $E_{bn}^{(i)}$ (in the initial version) or the ratio of times spent above these levels (in our version). In both versions, the interval between E_{bn} and $E_{bn} + \epsilon_{off}$ where the system equilibrium is strongly disturbed is excluded (see Fig. 11) in order to compute these ratios as correct as possible.

However, in spite of the exclusion of this interval, the introduction of artificial energy levels E_{bn} (and the prohibition to visit the phase space with $E < E_{bn}$) still leads to systematic errors by the computation of F_i 's. The reason for these errors is that the true thermal equilibrium is disturbed for all energies above E_{bn} . This perturbation can be demonstrated using the *normalized* probability histograms shown in Fig. 11(b). Here, it can be seen that for $E > E_{bn} + \epsilon_{off}$, the probability $\rho(E|E_{bn}^{(i)})$ is always *larger* compared to the true-equilibrium distribution $\rho(E)$ because for energies close to $E_{bn}^{(i)}$, the energy bounce histogram is *smaller* than the actual $\rho(E)$. This systematic deviation is different for different E_{bn} levels due to the energy dependence of the system density of states $D(E)$ (see Fig. 2). Hence, the coefficients F_i computed as ratio of any quantities derived from system trajectories above $E_{bn} + \epsilon_{off}$ also exhibit systematic deviation from the correct transfer coefficients.

The effect considered above is small because the main energy dependence of the probability $p(E)$ is due to the Boltzmann exponent $\exp(-E/k_B T)$, and not to the dependence $D(E)$. Still, this small effect, accumulated in course of subsequent multiplications of F_i 's, most probably leads to the above-mentioned systematic underestimation of the switching time by the energy bounce method.

In spite of this underestimation, the energy bounce method performs considerably better than the TTE method, leading for the highest studied barrier to the underestimation of τ_{sw} only by two times compared to the analytical approximation and three times to the forward-flux method.

Forward-flux sampling. Among all numerical methods considered here, the FFS is the only one which uses neither any far-reaching extrapolation from high- T results nor any artificial boundaries restricting the system motion in the phase space. All LD simulations in frames of FFS are conducted for an undisturbed system, so that the method should be as reliable as the LD itself. The only problem of FFS is the requirement to achieve a high accuracy by the evaluation of the transition probabilities between the interfaces $p(\lambda_{i+1}|\lambda_i)$. As explained above, we have solved this problem by positioning interfaces in the energy space and thus could obtain switching

times with a very low statistical error, as demonstrated in Fig. 21 (see yellow lines).

Switching times computed by FFS coincide with the LD results for low-energy barriers (within the statistical errors of the latter method). Further, $\tau_{\text{sw}}^{\text{FFS}}$ lie systematically above the analytical approximation (9), as it should be according to the consideration of back-hopping trajectories (see above).

The significance of the back-hopping processes for our system can be estimated from Fig. 20. Here, it can be seen that the probability to go downhill from the interface λ_7 (for which we have already $m_x < 0$, so that this interface is slightly beyond the barrier) is $\approx 90\%$, meaning that about 10% of trajectories starting at this interface, go back to the initial basin **A**. Further, probability to go downhill from the interface λ_8 is only slightly larger than 90%, so that again $\approx 10\%$ of trajectories go back from this interface to the basin **A**. Finally, we recall that the interface λ_7 is already beyond the barrier, so that some back hopping may occur between the separatrix and this interface (note that the back-hopping probability is larger for trajectories in the immediate vicinity of the saddle point). Hence, we can conclude that the fraction of back-hopping trajectories is significant (in any case much larger than 20%), which makes the systematic increase of the FFS switching time in Fig 21(b) over the analytical expression plausible.

Interestingly, the ratio $\tau_{\text{sw}}^{\text{FFS}}/\tau_{\text{sw}}^{\text{an}}$ is nearly constant (≈ 1.5) for a very broad interval of switching times considered here. It might be an indication that for the macrospin model, the fraction of trajectories which return to the initial basin after crossing once the saddle point depends only weakly on the energy barrier height.

VIII. CONCLUSION

In this paper we have studied the dependence of the switching time for a bistable biaxial magnetic particle in dependence of its in-plane size, which translates into the dependence on the energy barrier separating two energy minima. We have applied two analytical methods (a simple transition state theory leading to the Arrhenius law and the sophisticated approach based on the Melnikov-Meshkov solution of the Kramers problem for an arbitrary damping) and four numerical techniques (straightforward LD simulations, the time-temperature extrapolation method, the energy bounce method, and the forward-flux sampling).

Analyzing the results obtained by analytical methods, we have shown that the parameter which governs the transition from the low damping to the high damping regime is not the damping λ in the LLG equation by itself, but rather the product of λ and the reduced energy barrier $\Delta E/k_B T$. Taking into

account that the damping for a typical magnetic material used in applications is $\lambda \sim 0.01$ and the energy barrier required to achieve a stability during a macroscopic time interval is $\Delta E \sim 50k_B T$, we conclude that magnetization switching proceeds usually in the intermediate damping regime $\lambda \Delta E/k_B T \sim 1$. Our comparison of switching times obtained in the Arrhenius approximation and in the Melnikov-Meshkov formalism confirms this conclusion.

Comparison of numerical methods has shown that for low-to-moderate energy barriers ($\Delta E \leq 10k_B T$) where direct LD simulations are possible, results of all numerical methods agree within statistical errors. However, when the energy barrier height increases, the relation of switching times obtained by the TTE and by the energy bounce methods to $\tau_{\text{sw}}^{\text{an}}$ systematically decreases (the decrease is slower for the energy bounce method), so that for sufficiently high barriers the analytically computed switching time becomes larger than the numerical one. We could show that this artificial trend is the consequence of physical principles the corresponding methods are based on. Hence, the quality of results obtained by the TTE and energy bounce method is limited.

For the forward-flux sampling, our recipe for choosing the interfaces which are equidistant in the energy space (for the evaluation of transition probabilities p_i) has led to nearly interface-independent probabilities p_i without any *a posteriori* optimization, assuring the high accuracy by the computation of switching times. Corresponding values $\tau_{\text{sw}}^{\text{FFS}}$ coincide with LD results for low barriers and are higher than $\tau_{\text{sw}}^{\text{an}}$ for all energy barriers studied here, demonstrating that FFS represents a reliable technique for computing switching rate in magnetic systems, and that a very high accuracy can be potentially achieved by this method.

In this research, we have concentrated on the inherent properties of various techniques to study the escape of magnetic systems over energy barriers, and thus have performed our studies in frames of the macrospin approximation. For real applications, a full-scale micromagnetic framework is clearly necessary. The corresponding generalization of our techniques proposed in this paper, except of the TTE method, is highly nontrivial due to the contribution of other energy terms (mainly the exchange energy). This problem and its solution will be discussed in details in the forthcoming publication.

ACKNOWLEDGMENTS

Financial support of the Deutsche Forschungsgemeinschaft (German Research Society), DFG Project No. BE 2464/18-1 is greatly acknowledged.

-
- [1] L. Onsager and S. Machlup, *Phys. Rev.* **91**, 1505 (1953).
 - [2] D. Berkov, *J. Magn. Magn. Mater.* **186**, 199 (1998).
 - [3] W. E. W. Ren, and E. Vanden-Eijnden, *Phys. Rev. B* **66**, 052301 (2002).
 - [4] R. Dittrich, T. Schrefl, and H. Forster, *IEEE Trans. Magn.* **39**, 2839 (2003).
 - [5] H. Jonsson, G. Mills, and K. Jacobsen, Nudged elastic band method for finding minimum energy paths of transitions, in

Classical and Quantum Dynamics in Condensed Phase Simulations (World Scientific, Singapore, 1998), Chap. 16, pp. 385–404.

- [6] H.-B. Braun, *J. Appl. Phys.* **76**, 6310 (1994).
- [7] G. Fiedler, J. Fidler, J. Lee, T. Schrefl, R. L. Stamps, H. Braun, and D. Suess, *J. Appl. Phys.* **111**, 093917 (2012).
- [8] H. Kramers, *Physica (Amsterdam)* **7**, 284 (1940).
- [9] W. Coffey and Y. Kalmykov, *J. Appl. Phys.* **112**, 121301 (2012).

- [10] W. F. Brown Jr, *IEEE Trans. Magn.* **15**, 1196 (1979).
- [11] I. Klik and L. Gunther, *J. Stat. Phys.* **60**, 473 (1990).
- [12] V. Mel'nikov and S. Meshkov, *J. Chem. Phys.* **85**, 1018 (1986).
- [13] W. T. Coffey, D. A. Garanin, and D. J. McCarthy, Crossover formulas in the Kramers theory of thermally activated escape rates—application to spin systems, in *Advances in Chemical Physics*, edited by I. Prigogine and S. A. Rice (John Wiley & Sons, 2001), Vol. 117, p. 483.
- [14] P. M. Déjardin, D. S. F. Crothers, W. T. Coffey, and D. J. McCarthy, *Phys. Rev. E* **63**, 021102 (2001).
- [15] W. T. Coffey, D. S. F. Crothers, Y. P. Kalmykov, and J. T. Waldron, *Phys. Rev. B* **51**, 15947 (1995).
- [16] W. T. Coffey, D. S. F. Crothers, J. L. Dormann, L. J. Geoghegan, Y. P. Kalmykov, J. T. Waldron, and A. W. Wickstead, *Phys. Rev. B* **52**, 15951 (1995).
- [17] Y. P. Kalmykov, W. T. Coffey, B. Ouari, and S. V. Titov, *J. Magn. Magn. Mater.* **292**, 372 (2005).
- [18] A. Hubert, *Magnetic Domains: The Analysis of Magnetic Microstructures* (Springer, Berlin, 1998).
- [19] S. Wang and P. Visscher, *J. Appl. Phys.* **99**, 08G106 (2006).
- [20] R. Dittrich, T. Schrefl, A. Thiaville, J. Miltat, V. Tsiantos, and J. Fidler, *J. Magn. Magn. Mater.* **272–276**, 747 (2004).
- [21] A. Meo, P. Chureemart, S. Wang, R. Chepulskeyy, D. Apalkov, R. W. Chantrell, and R. F. L. Evans, *Sci. Rep.* **7**, 16729 (2017).
- [22] J.-H. Moon, T. Y. Lee, and C.-Y. You, *Sci. Rep.* **8**, 13228 (2018).
- [23] E. K. Semenova and D. V. Berkov, *AIP Adv.* **9**, 055307 (2019).
- [24] R. J. Allen, P. B. Warren, and P. R. ten Wolde, *Phys. Rev. Lett.* **94**, 018104 (2005).
- [25] R. J. Allen, D. Frenkel, and P. R. ten Wolde, *J. Chem. Phys.* **124**, 194111 (2006).
- [26] E. E. Borrero and F. A. Escobedo, *J. Chem. Phys.* **129**, 024115 (2008).
- [27] R. Allen, C. Valeriani, and P. R. ten Wolde, *J. Phys.: Condens. Matter* **21**, 463102 (2009).
- [28] C. Vogler, F. Bruckner, B. Bergmair, T. Huber, D. Suess, and C. Dellago, *Phys. Rev. B* **88**, 134409 (2013).
- [29] C. Vogler, F. Bruckner, D. Suess, and C. Dellago, *J. Appl. Phys.* **117**, 163907 (2015).
- [30] S. Wang and P. Visscher, *IEEE Trans. Magn.* **43**, 2893 (2007).
- [31] M. Chudnovsky, *J. Appl. Phys.* **73**, 6697 (1993).
- [32] B. Barbara and W. Wernsdorfer, *Curr. Opin. Solid State Mater. Sci.* **2**, 220 (1997).
- [33] J. Xue and R. Victora, *Appl. Phys. Lett.* **77**, 3432 (2000).
- [34] P. Haenggi, P. Talkner, and M. Borkovec, *Rev. Mod. Phys.* **62**, 251 (1990).
- [35] C. Kittel, *Phys. Rev.* **71**, 270 (1947).
- [36] E. Pollak, H. Grabert, and P. Hänggi, *J. Chem. Phys.* **91**, 4073 (1989).
- [37] L. J. Geoghegan, W. T. Coffey, and B. Mulligan, Differential recurrence relations for non-axially symmetric rotational fokker-planck equations, in *Advances in Chemical Physics* (Wiley, Hoboken, NJ, 2007), pp. 475–641.
- [38] S. Gardiner, *Handbook on Stochastic Processes* (Springer, Berlin, 1997).
- [39] D. Berkov, Magnetization dynamics including thermal fluctuations, in *Handbook of Magnetism and Advanced Magnetic Materials*, edited by H. Kronmüller and S. Parkin, Vol. 2 (Wiley, Hoboken, NJ, 2007), Chap. 4, pp. 795–823.
- [40] D. V. Berkov and N. L. Gorn, MICROMAGUS: package for micromagnetic simulations, <http://www.micromagus.de>
- [41] D. V. Berkov and N. L. Gorn, *J. Phys.: Condens. Matter* **14**, L281 (2002).
- [42] W. Press, S. A. Teukolsky, V. W. T., and B. P. Flannery, *Numerical Recipes in Fortran 77: The Art of Scientific Computing* (Cambridge University Press, Cambridge, 1992).